NASA TN D-1291

NASA TN D-1291

TECHNICAL NOTE

D-1291

SOLAR PROTON IMPACT ZONES

Thomas Kelsall

Goddard Space Flight Center
Greenbelt, Maryland

NATIONAL AERONAUTICS AND SPACE ADMINISTRATION
WASHINGTON
June 1962

G-182

SOLAR PROTON IMPACT ZONES

by
Thomas Kelsall
Goddard Space Flight Center

SUMMARY

The trajectories of charged particles moving in a magnetic dipole field have been calculated by numerical integration for application to data on the intensity variation of cosmic rays during recent solar events. All seasons and times of day have been covered by assuming a range of orientations of the incident particle beam with respect to the magnetic dipole axis. The points of impact with the earth have been determined for protons with energies from 0.05 to 50 Bev. The computation includes 4000 trajectories and fills several gaps in previous investigations. In agreement with earlier calculations the results indicate that the protons strike in well defined areas between 0 and 1200 hours local time and are focused into small areas of impact at low energies.

The investigation has shown two facts which are not new, but which have received relatively little attention in earlier work. First, the relative number of impacts in the northern and southern geomagnetic hemispheres is strongly dependent on season. Second, under certain conditions of season there is a class of trajectories which may be called quasi-trapped, consisting of a set of paths which resemble the trapped trajectories first discovered by Störmer but which are connected to infinity. It is suggested that injection into trapped orbits from these quasi-trapped trajectories may make a contribution to the population of the Van Allen belts.

CONTENTS

Summary i
INTRODUCTION 1
CALCULATION OF TRAJECTORIES 2
RESULTS 7
ACKNOWLEDGMENTS 32
References 32

SOLAR PROTON IMPACT ZONES*†

by
Thomas Kelsall
Goddard Space Flight Center

INTRODUCTION

In the past two decades five large solar flares associated with cosmic ray increases have been reported. These flares occurred on February 28 and March 7, 1942; July 25, 1946; November 19, 1949; and February 23, 1956. (A cosmic ray increase also accompanied the class 3+ flare of November 10-12, 1960.) The increase in cosmic ray intensity was usually noted about an hour after an optical flare was sighted. The intensity rose sharply during the first few minutes and decayed within several hours.

The cosmic ray increases were world-wide, but their amplitude and time of onset exhibited a longitudinal dependence. The integral rigidity spectrum of the flare particles was much steeper than that of galactic cosmic rays. In an effort to explain the ground level pattern of the cosmic ray increases observed during these solar events, several investigations have been performed (References 1 through 8) in which Störmer trajectories were computed for cosmic rays originating at the sun and moving in the earth's dipole field. Laboratory models have also been constructed for this problem. Birkeland (Reference 9) constructed the first such model, in which a fluorescent-coated magnetized sphere, called the terrella, was exposed to a stream of electrons in an evacuated chamber. The regions of electron impact fluoresced and were photographed. More advanced experiments have been performed by Malmfors (Reference 10), Brunberg and Dattner (Reference 11), and Bennett (Reference 12).

The present investigation extends the earlier theoretical studies on impact zones. The calculation includes orientations of the proton beam and dipole axis covering all possible conditions of season and time of day. Points of impact are determined for protons with energies ranging from 0.05 to 50 Bev.

*Much of this work was done while the author was at the Naval Research Laboratory, Washington, D. C. Part of this work was submitted to George Washington University in partial fulfillment of the requirements for the degree of Master of Science.

†This report has also been published in J. Geophys. Res 66(12):4047-4070, December 1961

The results confirm earlier work indicating well-defined impact areas lying between 0 and 1200 hours local time and diminishing in size with decreasing proton energy. Protons of relatively low energy, in the order of 1 Bev or less, are strongly focused by the magnetic field into impact zones of very limited size. The calculations also demonstrate a strong seasonal dependence in the ratio of impacts in the northern and southern geomagnetic hemispheres.

Finally, for certain conditions of season and time of day, there are particle trajectories which approach the earth and make several passes about it, in the manner of the Van Allen belt particles, before receding again to infinity. This class of quasi-trapped particles perturbed by scattering may be a source of protons for the Van Allen layers.

CALCULATION OF THE TRAJECTORIES

The Lorentz force acting on a particle of charge q and velocity v in a magnetic field of strength H is

$$\vec{F} = \frac{q}{c} \vec{v} \times \vec{H} . \tag{1}$$

For a dipole field

$$\vec{H} = \frac{3\vec{r}\,\vec{M}\cdot\vec{r} - \vec{M}r^2}{r^5} , \tag{2}$$

where $\vec{M}$ is the dipole moment and $\vec{r}$ the position vector.

The magnetic force on a particle is transverse to its motion and can do no work; hence the energy and the magnitude of the velocity are constants of the motion. It is possible, then, to replace the increment in time by an increment in arc length:

$$dt = \frac{dS}{v} . \tag{3}$$

If Equation 1 is expanded by using Equations 2 and 3 and taking z antiparallel to the dipole axis, then

$$\frac{d^2x}{dS^2} = x'' = \frac{Mq\left[(x^2 + y^2 - 2z^2)\,y' + 3yzz'\right]}{mcvr^5} ,$$

$$\frac{d^2y}{dS^2} = y'' = \frac{Mq\left[(2z^2 - x^2 - y^2)\,x' - 3xzz'\right]}{mcvr^5} ,$$

and

$$\frac{d^2z}{dS^2} = z'' = \frac{3Mqz\,(xy' - yx')}{mcvr^5} ,$$

where m is the relativistic mass of the particle. As Mq/mcv has the dimensions of (length)^2, it is convenient to introduce the Störmer unit of length,

$$\text{S. U.} = \left(\frac{Mq}{mcv}\right)^{\frac{1}{2}} . \tag{4}$$

The dipole field is invariant for rotations about the z axis; thus, the z component of the canonical angular momentum h is a constant (Reference 13):

$$h = (xy' - yx') - \frac{(x^2 + y^2)}{r^3} . \tag{5}$$

The final form of the equations used in the integration is

$$\left.\begin{aligned} x'' &= \frac{\left[(x^2 + y^2 - 2z^2)\,y' + 3yzz'\right]}{r^5} , \\ y'' &= \frac{\left[(2z^2 - x^2 - y^2)\,x' - 3xzz'\right]}{r^5} , \\ z'' &= 3z\left[\frac{h}{r^5} + \frac{x^2 + y^2}{r^8}\right] . \end{aligned}\right\} \tag{6}$$

The calculations are made for a stream of protons ejected from the sun during a flare. The protons in the beam are assumed to be moving parallel to the plane of the ecliptic when they reach the earth's orbit and are assumed to be without internal interactions. Each trajectory is designated by its coordinates in a plane perpendicular to the direction of the proton beam (plane A B in Figure 1) and with its center located six Störmer units from the center of the dipole at geomagnetic longitude zero and colatitude ninety. Coordinates a and b in this plane are oriented respectively in the ecliptic and perpendicular to it. A trajectory is integrated numerically from a starting point in the A B plane.

The initial conditions for a proton striking the A B plane perpendicularly at a point $P(a, b)$ are, from Figure 1,

$$\left.\begin{aligned} x_0 &= 6 \sin\alpha - b\cos\alpha , \\ y_0 &= -a , \\ z_0 &= 6\cos\alpha + b\sin\alpha ; \end{aligned}\right\} \tag{7}$$

and

$$\left.\begin{aligned} x'_0 &= -\sin\alpha, \\ y'_0 &= 0, \\ z'_0 &= -\cos\alpha, \end{aligned}\right\} . \tag{8}$$

The integration interval ΔS is defined by

$$\Delta S = \begin{cases} 0.2 \text{ if } 0.2 \leq 0.02\,\bar{C}^{-1} \\ 0.02\,\bar{C}^{-1} \text{ if } 0.2 > 0.02\,\bar{C}^{-1} \end{cases} .$$

Here $\bar{C}$ is the curvature

$$\bar{C} = \left[(x'')^2 + (y'')^2 + (z'')^2\right]^{\frac{1}{2}} . \tag{9}$$

At each step of the integration the identity

$$E = 1 = (x')^2 + (y')^2 + (z')^2 \tag{10}$$

is checked. If E deviates from 1 by ± 1.5 percent, the computation halts and an error check is printed out. The integration is usually terminated when $\bar{C} \leq 10^{-2}$ and is less than

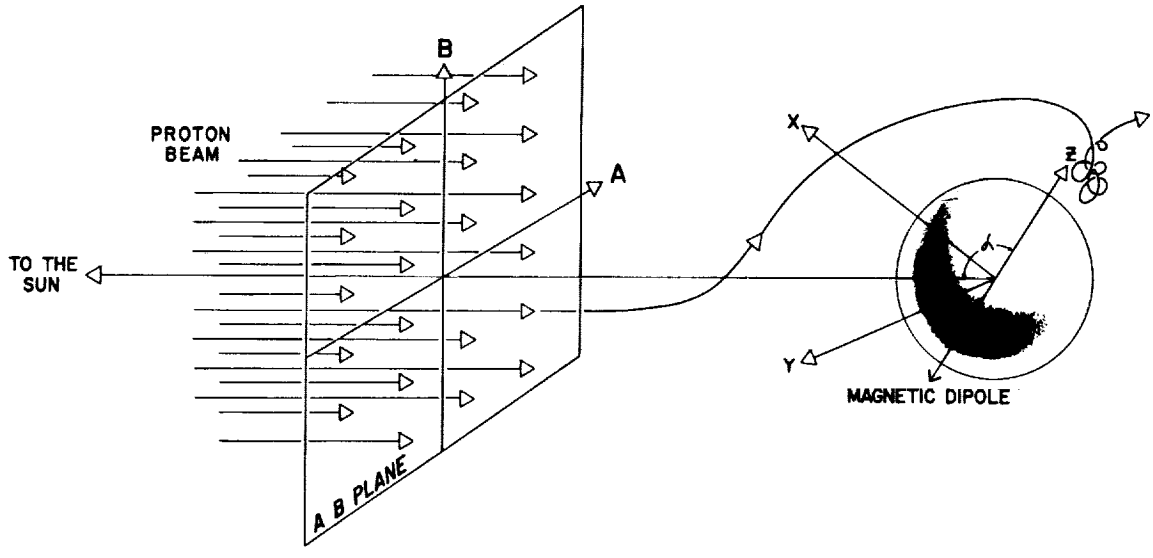

Figure 1 - Schematic of the geometry of the problem

the previously calculated $\bar{C}$. This condition on $\bar{C}$ represents the escape of the proton from the magnetic field.

The numerical integration of Equation 6, using the fourth order Runge-Kutta method, was done on the NORC computer at the Naval Proving Grounds in Dahlgren, Virginia, and on the IBM 704 computer at the National Bureau of Standards in Washington, D. C.

The machine output is printed in the following format: (1) a first line of a, b, α, and h; (2) lines of E, S, x, y, z, r^2, dS, $\vec{C}^2$, where dS is the computed distance (in Störmer units) which has been traversed between successive lines of printing; and (3) a last line of E, x, y, z, x', y', and z'. Since the Störmer unit is energy dependent, the earth's radius r_0 differs for each proton energy (see Table 1).

Table 1

Corresponding Values of Energy, Rigidity, Velocity, Störmer Units, and r_0 for Protons

Energy (Bev)	Rigidity (10^6 gauss-cm)	Velocity (10^{10} cm/sec)	Störmer Unit (10^9 cm)	r_0 Radius of the Earth in Störmer Units
50	170	3.00	0.69	0.922
25	86.5	3.00	0.97	0.658
10	36.4	2.99	1.49	0.427
5.0	19.6	2.96	2.04	0.313
2.5	11.0	2.88	2.71	0.235
1.0	5.65	2.62	3.78	0.168
0.50	3.64	2.27	4.72	0.135
0.25	2.43	1.84	5.77	0.110
0.10	1.48	1.28	7.40	0.086
0.05	1.03	0.94	8.85	0.072

When in the integration a value of r is reached for the first time which is equal to an r_0 for some proton energy, the regular trajectory printing is interrupted by the printing of the special function lines. These special lines give: the Cartesian coordinates and velocity components at the point of impact; the point's geomagnetic longitude ϕ and colatitude θ; and the angle of impact of the proton with respect to the local zenith ψ. Special lines are printed for r's representing protons with energies of 0.05, 0.10, 0.25, 0.5, 1.0, 2.5, 5, 10, 25 and 50 Bev.

The field is represented by an earth-centered dipole, of moment 8.1×10^{25} Gauss-cm^3, with its axis inclined to the axis of rotation by 11.5 degrees. The dipole's angular orientation with respect to the earth-sun line varies with the time of day and of year. The variation in the angular orientation of the rotation axis with respect to the ecliptic is between 90 ± 23.5 degrees during a year; thus, the dipole axis will vary between 90 ± 35 degrees. The envelopes of diurnal variation of the dipole's angle of inclination α versus season are shown in Figure 2. Proton trajectory calculations were performed covering the range in α from 90 to 125 degrees in five steps: α = 90, 100, 110, 117, and 125 degrees. The calculations were made only for $\alpha \geq 90$ degrees as equal variations of α about 90 degrees are equivalent from the equatorial and rotational symmetry of the dipole field. For example, the trajectory and associated impact points calculated for α = 110 degrees equal those for α = 70 degrees if the hemispheres are interchanged, that is $z \rightarrow -z$.

Consideration of proton penetrability into the upper atmosphere limited the detailed analysis to protons with impact angle $\leq$ 45 degrees.

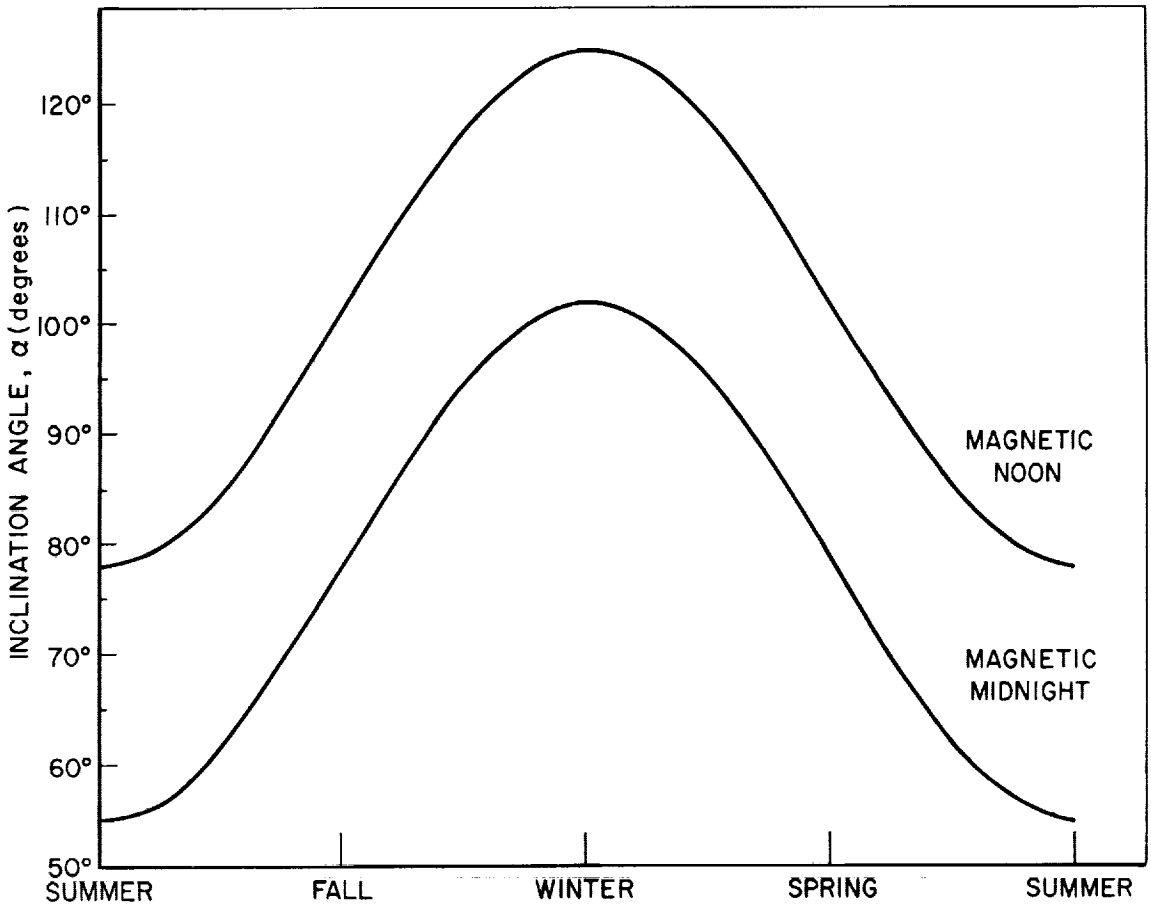

Figure 2 - Seasonal dependence of the extremes (magnetic noon and magnetic midnight) in the diurnal variation of the dipole's inclination angle α

The spacing of points required for the detailed analyses in the AB plane decreases with decreasing proton energy. Table 2 lists, for the various proton energies and values of α, areas in the AB plane and the number of trajectory starting points enclosed within each area.

Table 2

Number of Trajectories Enclosed in the Net Area Used in Spanning the AB Plane for Proton Energies and Angles of α of Interest

Proton Energy (Bev)	Number of Trajectories Per net Area $\left(\frac{\text{Number}}{(\text{Störmer Units})^2}\right)$				
	$\alpha = 90°$	$\alpha = 100°$	$\alpha = 110°$	$\alpha = 117°$	$\alpha = 125°$
50	$4/(0.1)^2$	$4/(0.1)^2$	$4/(0.1)^2$	$4/(0.1)^2$	$4/(0.1)^2$
25	"	"	"	"	"
10	$4/(0.05)^2$	$4/(0.05)^2$	$5/(0.05)^2$	$4/(0.05)^2$	$4/(0.05)^2$
5.0	"	"	"	"	"
2.5	$4/(0.025)^2$	$4/(0.025)^2$	"	"	"
1.0	"	"	"	"	"
0.50	"	"	"	"	"
0.25	"	"	"	"	"
0.10	"	"	"	"	"
0.05	"	"	"	"	"

The centered dipole approximation appears to be good far above the surface as indicated by the form of the Van Allen belts and recent rocket-flown magnetometer data. For a more accurate description near the surface, neutron monitoring experiments (References 14 and 15) indicate that the higher harmonics should be taken into account.

RESULTS

The impact zones on the earth's surface were determined as a result of 4000 separate trajectory calculations covering the five values of α. The parameters were chosen for protons, but the results can be applied to any charged particle. Table 3 lists three primary particles (proton, electron, alpha particle) and the corresponding values of energy for which the results are valid.

Table 3

Corresponding Energy Values of Protons, Electrons, and Alpha Particles for a Given Magnetic Rigidity and r_0

Magnetic Rigidity (10^6 gauss-cm)	r_0 Radius of the Earth (Störmer Units)	Proton Energy (Bev)	Electron Energy (Bev)	Alpha Particle Energy (Bev)
170	0.922	50.0	50.9	98.2
84.5	0.658	25.0	25.9	48.2
36.4	0.427	10.0	10.9	18.4
19.6	0.313	5.0	5.86	8.5
11.0	0.235	2.50	3.31	3.86
5.66	0.168	1.00	1.70	1.31
3.64	0.135	0.500	1.09	0.591
2.43	0.110	0.250	0.729	0.276
1.48	0.086	0.100	0.444	0.105
1.04	0.072	0.050	0.310	0.052

For negatively charged particles, interchange the hemispheres in all tabulations and figures giving impact zones.

The surface impact points for protons can be transformed to any height above the earth by an appropriate shift in the proton energy. Table 4 lists the changes in proton energy required to transform the results to altitudes of 50, 100 and 250 km.

Figures 3 through 7 show lines, each designated by a proton energy (Bev), in the AB planes which enclose the area from which protons with the specified energy come in and strike the earth with impact angles ranging from 0 to 90 degrees. The origin of the protons striking the earth is predominantly the first and fourth quadrants of the AB plane, because the $\vec{v} \times \vec{H}$ force tends to twist the protons clockwise, looking down on the ecliptic plane. Since the measure of length in Figures 3 through 7 is the Störmer units, it is difficult to estimate the actual contributing areas for the various energies.

Column A of Table 5 gives the areas in the AB plane in square kilometers. The table shows that the contributing areas for protons with energies of 25 Bev or more decrease with increasing α, but for lower energies no clear relationship is obvious. The integrated area associated with earth-striking low energy ($\leq$ 10 Bev) protons peaks at α = 107 degrees.

Rough estimates of the areas of the impact zones on the earth's surface are listed in column B.

Table 4
Proton Energies Which Transform the Impact Zones on the Earth to Specific Heights Above the Surface

Proton Striking Energy (Bev)	Proton Energies for Specified Heights above the Surface (Bev)		
	50 km	100 km	250 km
50.0	49.2	48.3	46.1
25.0	24.6	24.2	23.1
10.0	9.84	9.66	9.19
5.00	4.92	4.84	4.56
2.50	2.44	2.41	2.25
1.00	0.970	0.948	0.884
0.500	0.487	0.474	0.439
0.250	0.241	0.234	0.216
0.100	0.096	0.093	0.086
0.050	0.049	0.047	0.043

Table 5
Areas Covered on the AB Plane and on the Earth by Protons with Impact Angles $\leq 45°$ for the Various Values of α

Proton Energy (Bev)	$\alpha = 90°$			$\alpha = 100°$			$\alpha = 110°$		
	A*	B*	C*	A	B	C	A	B	C
50	87	93	0.94	87	97	0.90	74	81	0.91
25	150	100	1.5	130	82	1.6	82	53	1.6
10	47	26	1.8	57	29	1.9	66	29	2.3
5.0	40	6.1	6.6	35	2.7	13	49	2.6	19
2.5	25	0.40	62	24	0.41	57	44	0.76	57
1.0	16	0.049	320	17	0.091	180	45	0.13	350
0.50	7.0	0.021	340	14	0.023	610	40	0.12	320
0.25	6.2	0.004	1600	8.3	0.012	680	18	0.052	350
0.10	6.8	0.002	3800	4.3	...	...	3.8	...	...
0.05	4.9	...	...	1.8	...	...	0.0	...	...

Proton Energy (Bev)	$\alpha = 117°$			$\alpha = 125°$		
	A	B	C	A	B	C
50	65	73	0.90	54	55	0.99
25	38	25	1.5	27	17	1.6
10	31	6.8	4.5	13	0.52	26
5.0	9.1	0.64	14	9.3	0.54	17
2.5	6.9	0.035	190	6.9	0.059	120
1.0	5.2	0.015	350	4.5	0.013	340
0.50	4.5	0.007	630	3.7	0.002	1700
0.25	3.6	0.004	830	2.9	0.003	1100
0.10	1.7	...	...	2.9	...	...
0.05	0.92	...	...	1.5	...	...

*A = Area in the AB plane (10^6 km^2);
B = Area on the Earth (10^6 km^2); and
C = Ratio of A to B.

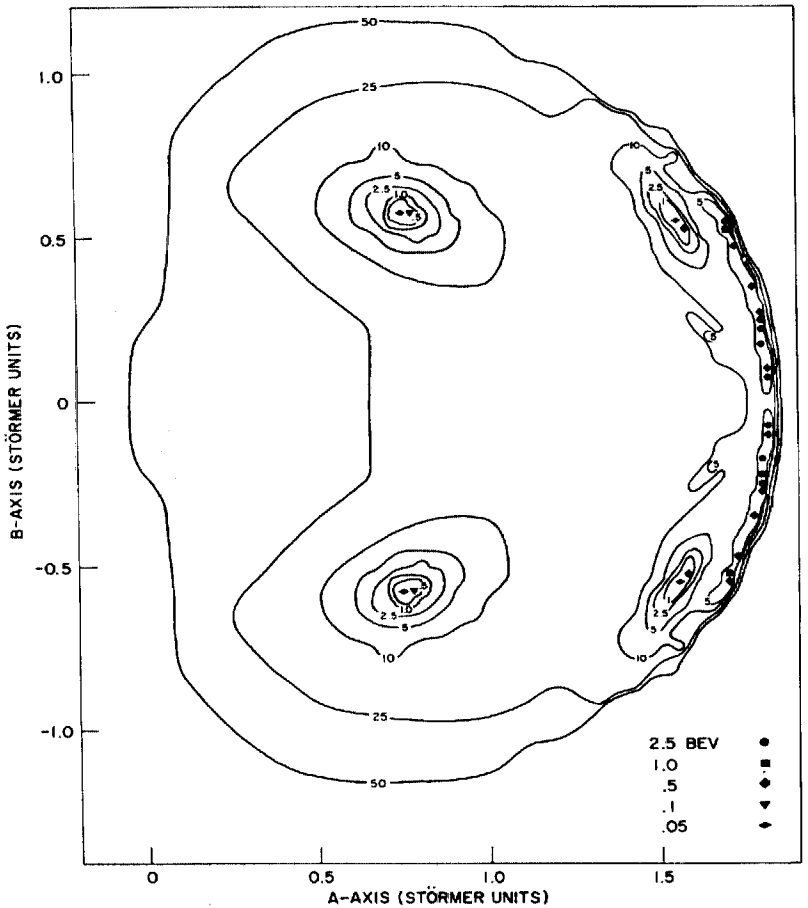

Figure 3 - Areas in the AB plane contributing earth-striking particles with impact angles ≤ 90° and with the energies shown on the boundries. Origins of low energy trajectories are shown as points.
α = 90° (See also Figures 4, 5, 6, and 7.)

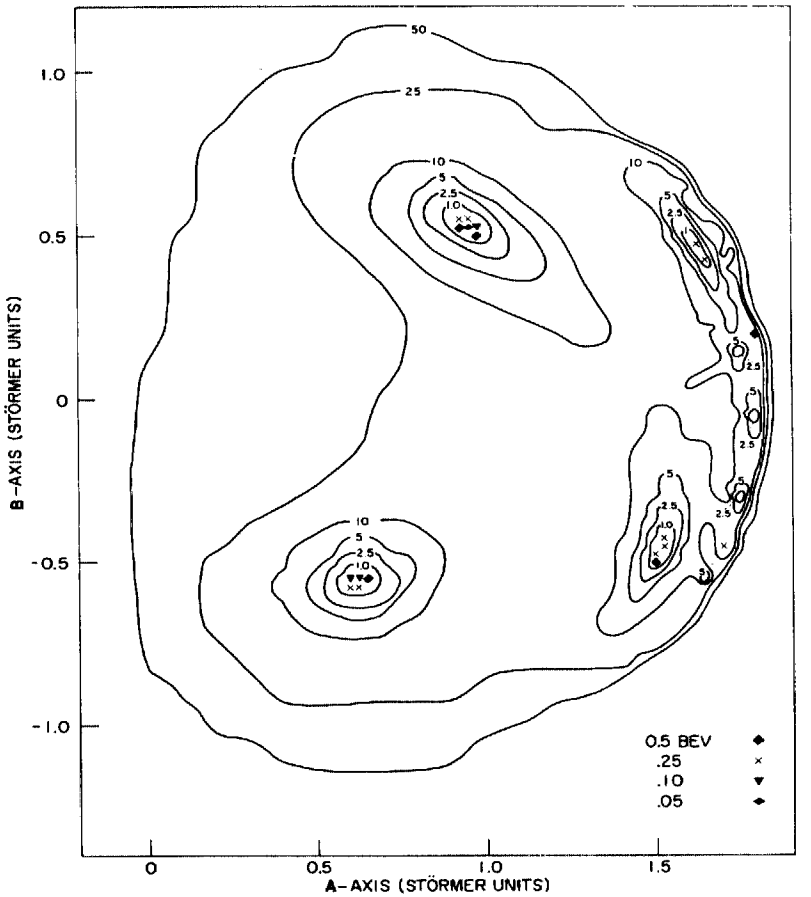

Figure 4 - Areas in the AB plane contributing earth-striking particles with impact angles ≤ 90° and with the energies shown on the boundries. Origins of low energy trajectories are shown as points.
α = 100° (See also Figures 3, 5, 6, and 7.)

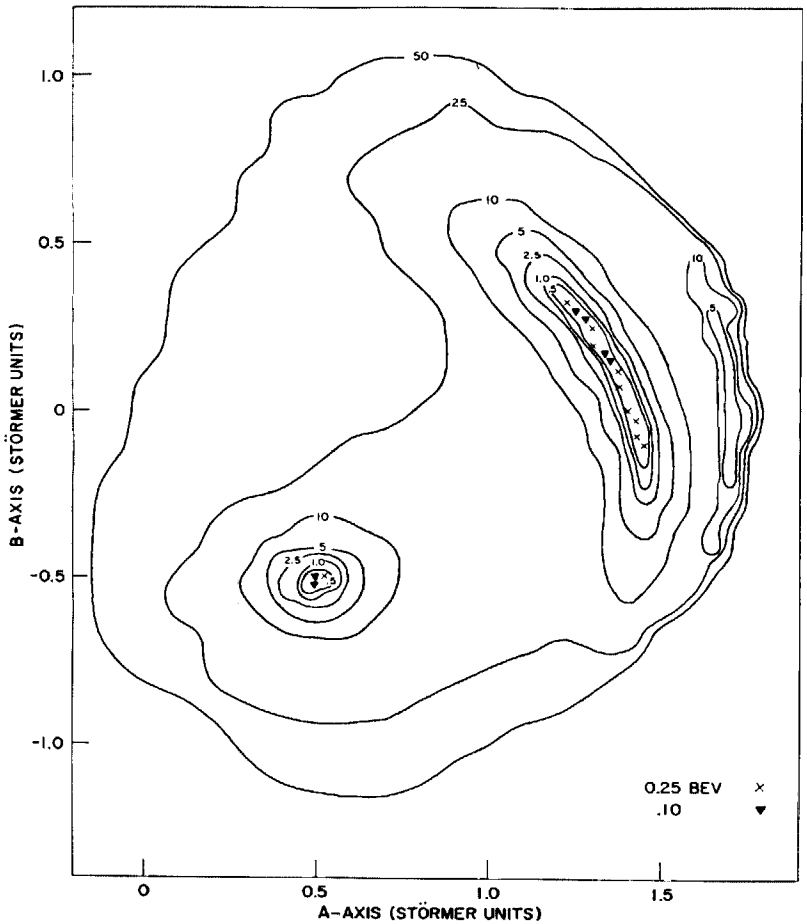

Figure 5 - Areas in the AB plane contributing earth-striking particles with impact angles ≤ 90° and with the energies shown on the boundries. Origins of low energy trajectories are shown as points.
α = 110° (See also Figures 3, 4, 6, and 7.)

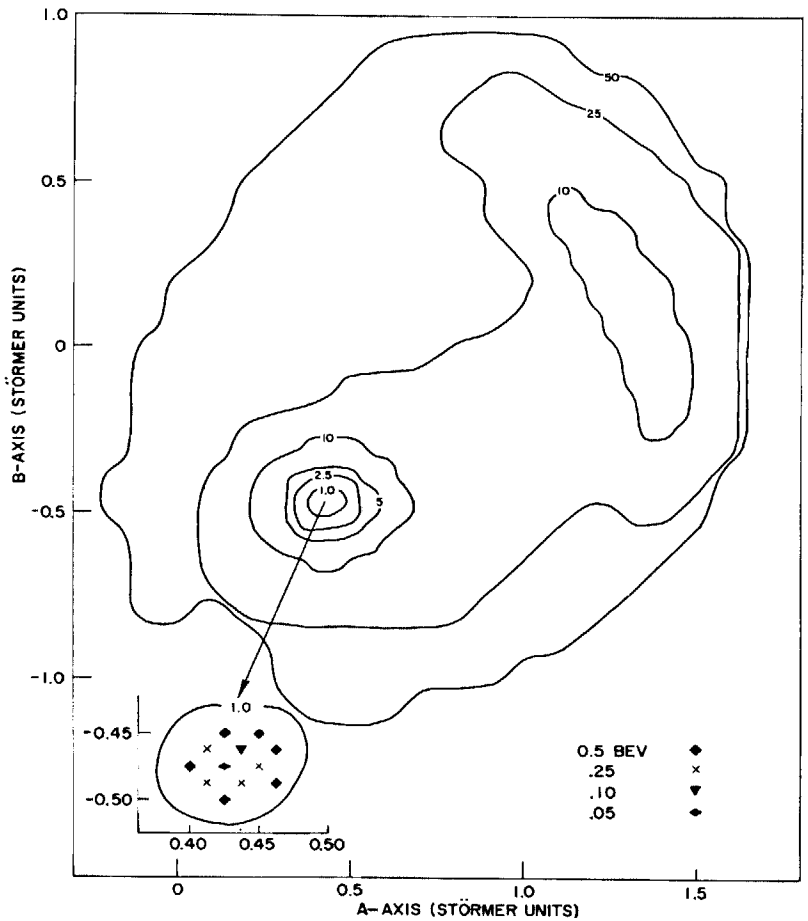

Figure 6 - Areas in the AB plane contributing earth-striking particles with impact angles ≤ 90° and with the energies shown on the boundries. Origins of low energy trajectories are shown as points.
α = 117° (See also Figures 3, 4, 5, and 7.)

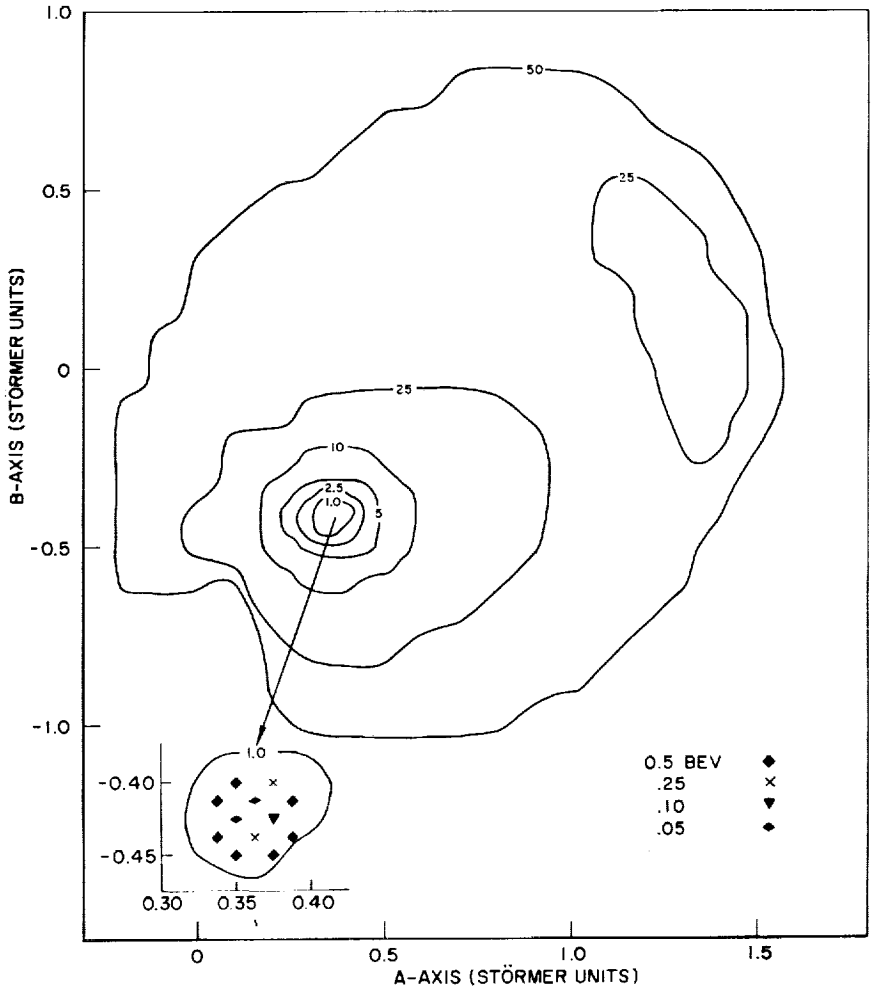

Figure 7 - Areas in the AB plane contributing earth-striking particles with impact angles $\leq 90°$ and with the energies shown on the boundries. Origins of low energy trajectories are shown as points.
$\alpha = 125°$ (See also Figures 3, 4, 5, and 6.)

Column C of Table 5 gives the ratio of the AB area to the area of the impact zone. This ratio is a measure of the focusing of incoming protons by the geomagnetic field. The pronounced focusing at low energies was first noticed by Birkeland (Reference 9) in his terrella experiments, and by Lüst (Reference 8) and Jory (Reference 7) in their calculations. The focusing of the low energy group is strongest for α = 117 and 125 degrees. At other angles the low energy contribution from areas along the edge and upper quadrant of the AB plane is scattered over a considerable region of the earth. When α = 117 and 125 degrees, the contributing area for the low energies is the lower left corner of the fourth quadrant, which exhibits particularly strong focusing. Two illustrative trajectories from this group are shown in Figure 8. A collection of such strongly focused spiraling trajectories may be a source of various local disturbances.

G-182

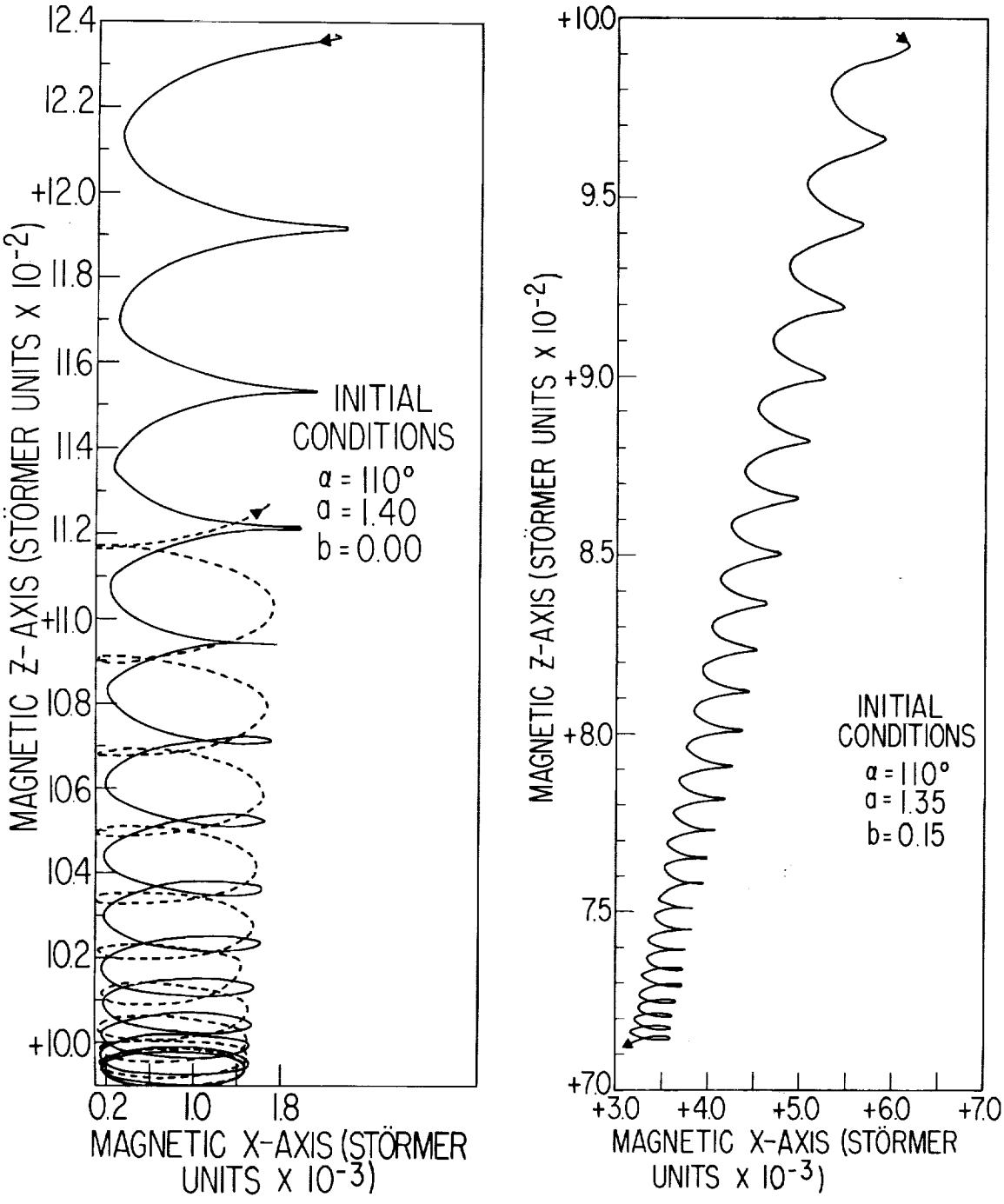

Figure 8 - Two examples of strongly focused protons spiraling in about a line of force

The systematic variation of the angle of impact for high energy protons along a line of a constant b is shown in Figure 9.

Figures 10 through 17 show the areas within which various energy groups will strike the earth's surface. All impact angles are included in these figures. Tables 6 through 14 list, for the five values of α the counting rates of protons with impact angles $\leq$ 45 degrees, in arbitrary units for the ten specified energies, in blocks on the earth's surface 10 degrees geomagnetic colatitude by 10 degrees geomagnetic longitude. In the construction of these tables all energies are given equal weight. In addition, the numbers have been normalized so that comparisons between different values of α are permissible. For α = 90 degrees protons lying in the ecliptic plane, originating along b = 0, will strike along the magnetic equator; these have been counted as striking in the southern hemisphere. The number of equatorial impacts can be deduced from Table 7, which lists the counting rates in the interval of colatitude 90 to 100 degrees only.

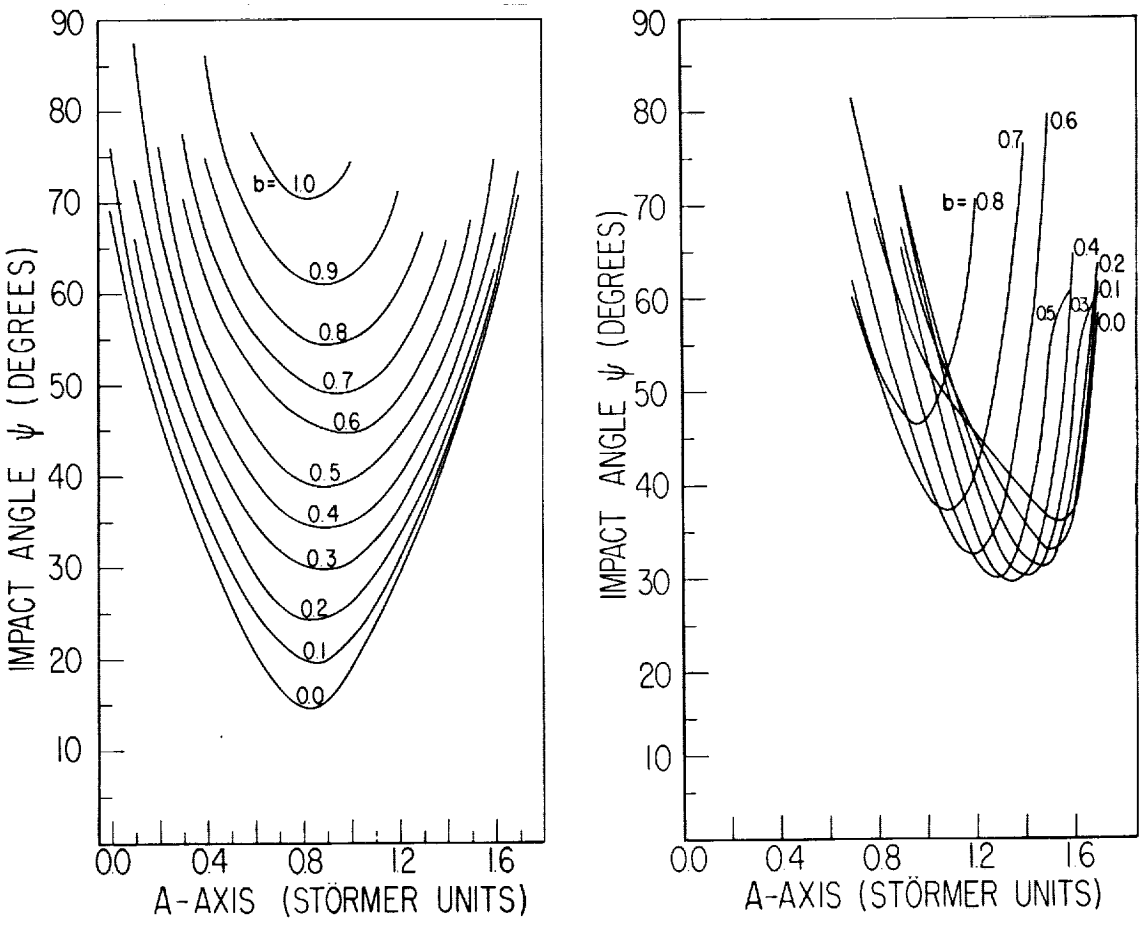

Figure 9 - The variation of impact angle with location in the AB plane for (left) 50 Bev and (right) 25 Bev protons; $\alpha = 110°$

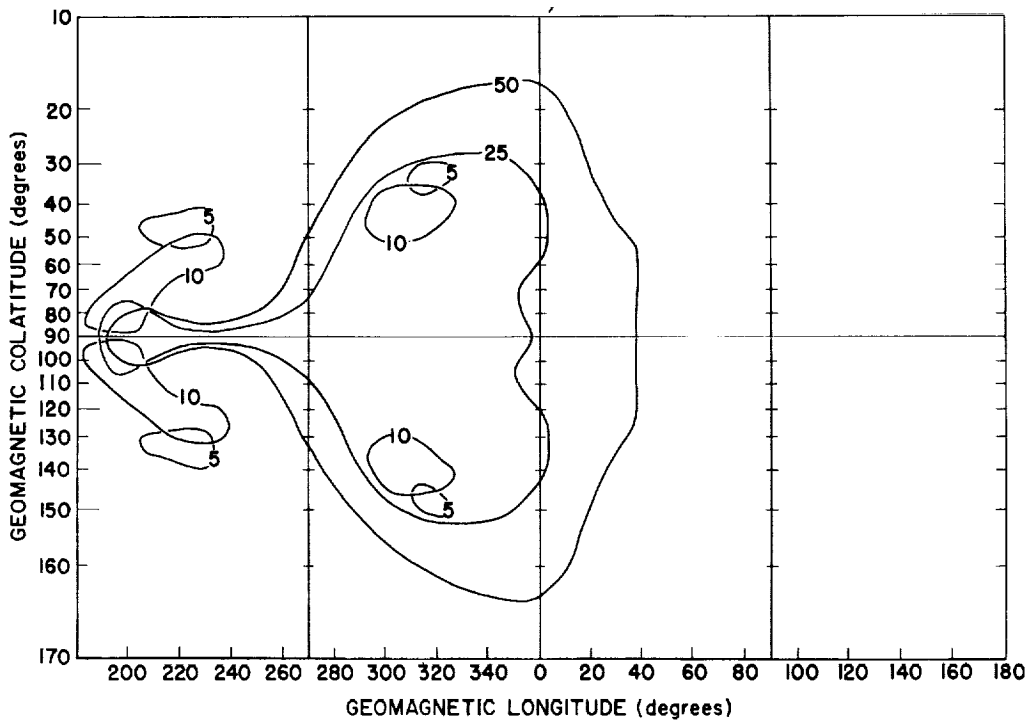

Figure 10 - Impact zones on the earth's surface for 50, 25, 10, and 2.5 Bev protons with impact angle $\psi \leq 90°$ when the dipole's angle of inclination $\alpha = 90°$. Local noon is at 0 degrees longitude. The map is a Mercator Projection with geomagnetic coordinates. (See also Figures 11, 12, 13, and 14.)

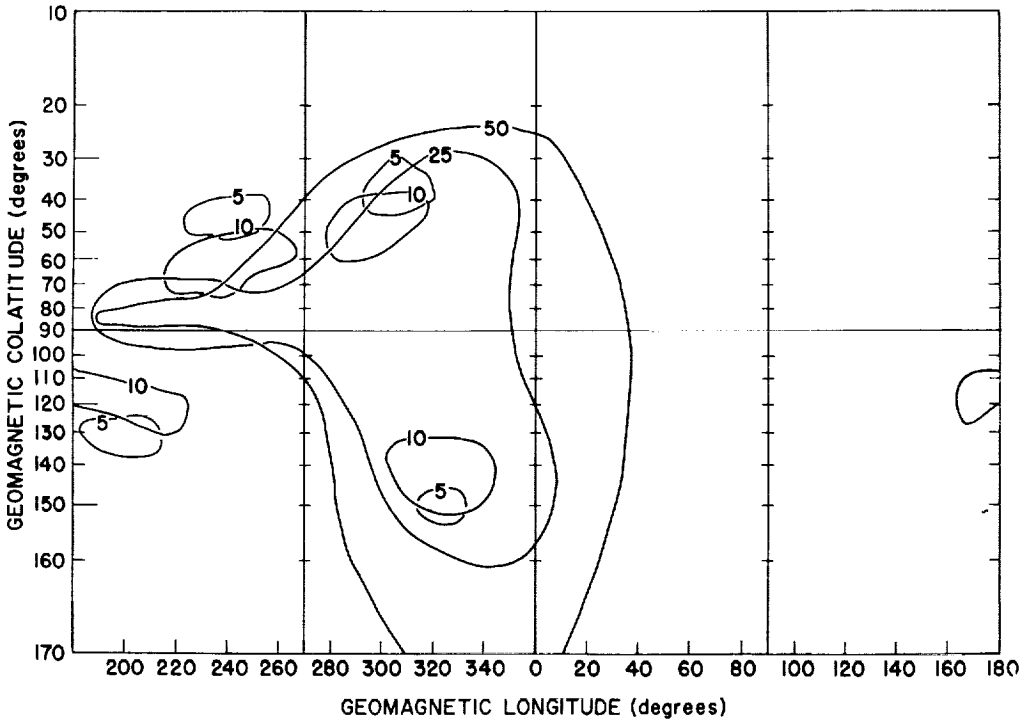

Figure 11 - Impact zones on the earth's surface for 50, 25, 10, and 2.5 Bev protons with impact angle $\psi \leq 90°$ when the dipole's angle of inclination $\alpha = 100°$. Local noon is at 0 degrees longitude. The map is a Mercator Projection with geomagnetic coordinates. (See also Figures 10, 12, 13, and 14.)

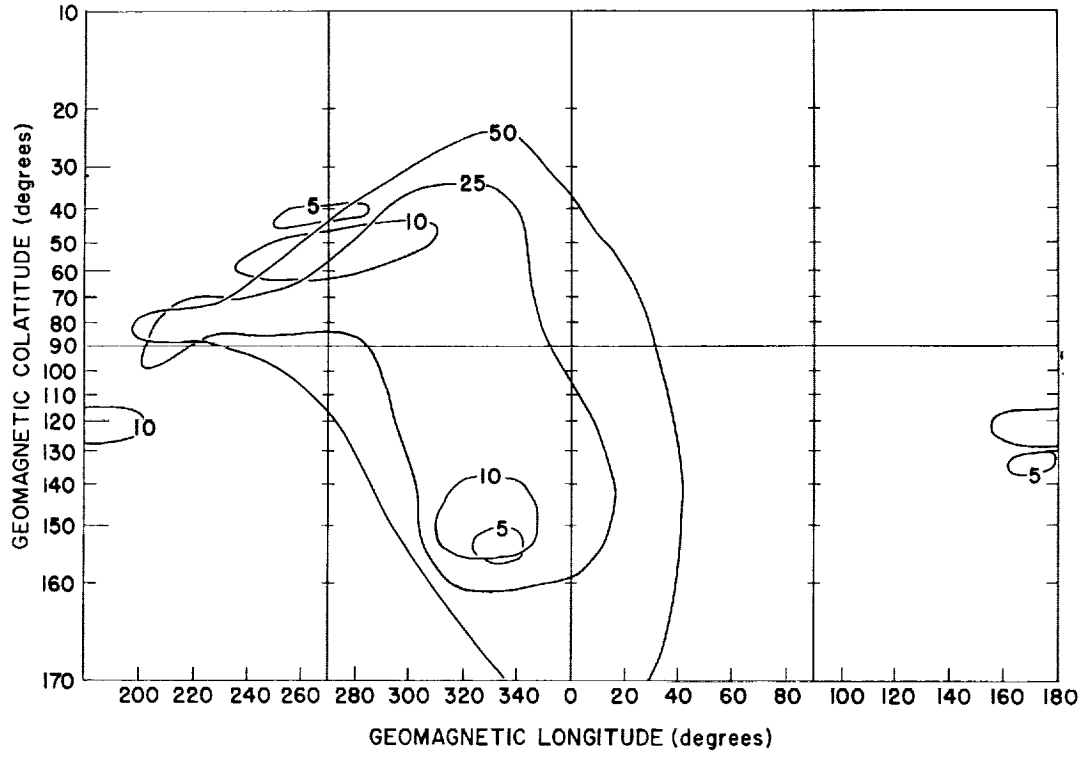

Figure 12 - Impact zones on the earth's surface for 50, 25, 10, and 2.5 Bev protons with impact angle $\psi \leq 90°$ when the dipole's angle of inclination $\alpha = 110°$. Local noon is at 0 degrees longitude. The map is a Mercator Projection with geomagnetic coordinates. (See also Figures 10, 11, 13, and 14.)

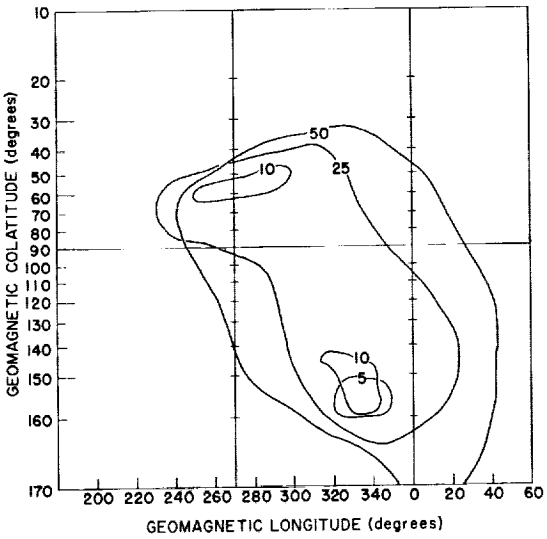

Figure 13 - Impact zones on the earth's surface for 50, 25, 10, and 2.5 Bev protons with impact angle $\psi \leq 90°$ when the dipole's angle of inclination $\alpha = 117°$. Local noon is at 0 degrees longitude. The map is a Mercator Projection with geomagnetic coordinates. (See also Figures 10, 11, 12, and 14.)

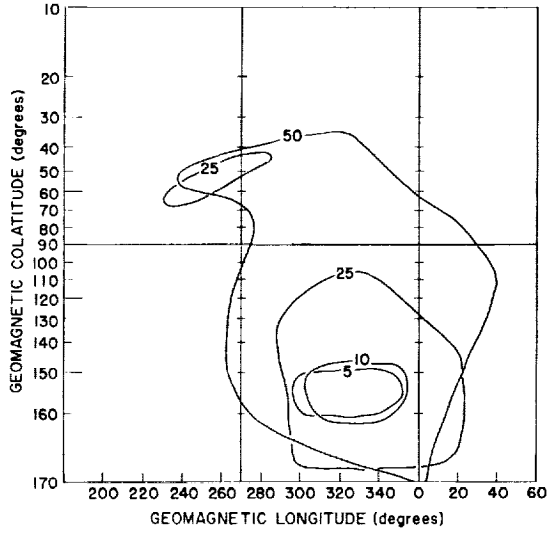

Figure 14 - Impact zones on the earth's surface for 50, 25, 10, and 2.5 Bev protons with impact angle $\psi \leq 90°$ when the angle of inclination $\alpha = 125°$. Local noon is at 0 degrees longitude. The map is a Mercator Projection with geomagnetic coordinates. (See also Figures 10, 11, 12, and 13.)

Figures 12 through 19 and Tables 6 through 14 indicate that ground observers would detect different counting rates depending on their location.

In Figures 20 and 21 the daily flux integrated over the earth is plotted against season for two different energy spectra of the beam.

Figures 22 through 25 plot the three major groups of trajectories: (1) trajectories which approach the day side of the earth, and return to infinity; (2) trajectories which approach the night side and return to infinity; (3) quasi-trapped trajectories which stay in the vicinity of the earth for a number of close passes before returning to infinity.

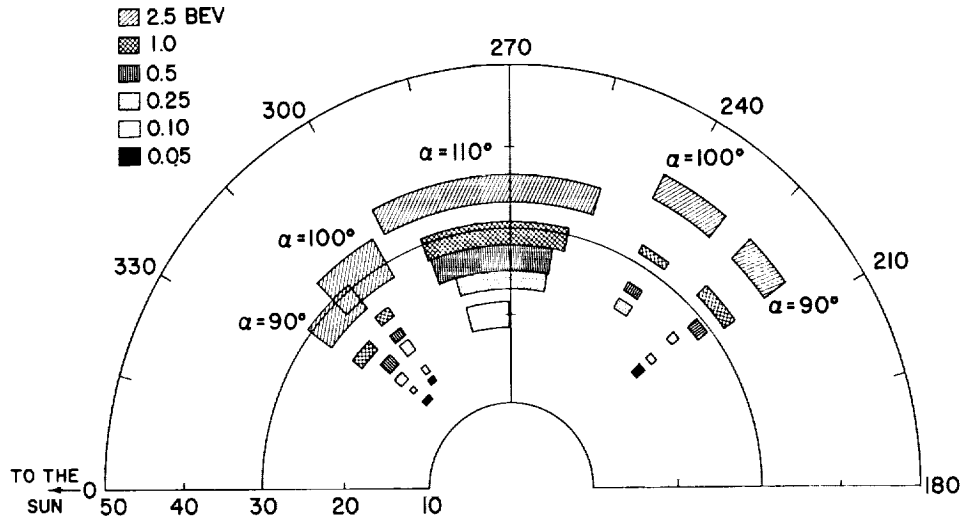

Figure 15 - Impact zones in the Northern Geomagnetic Hemisphere for 0.05 through 2.5 Bev protons when the impact angle $\psi \leq 90°$. (See also Figures 16 and 17.)

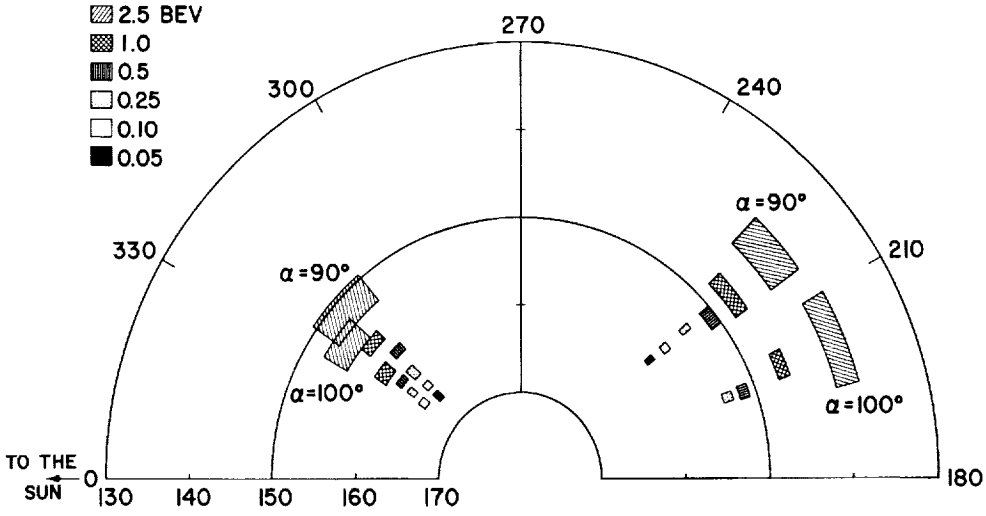

Figure 16 - Impact zones in the Southern Geomagnetic Hemisphere for 0.05 through 2.5 Bev protons when the impact angle $\psi \leq 90°$. (See also Figures 15 and 17.)

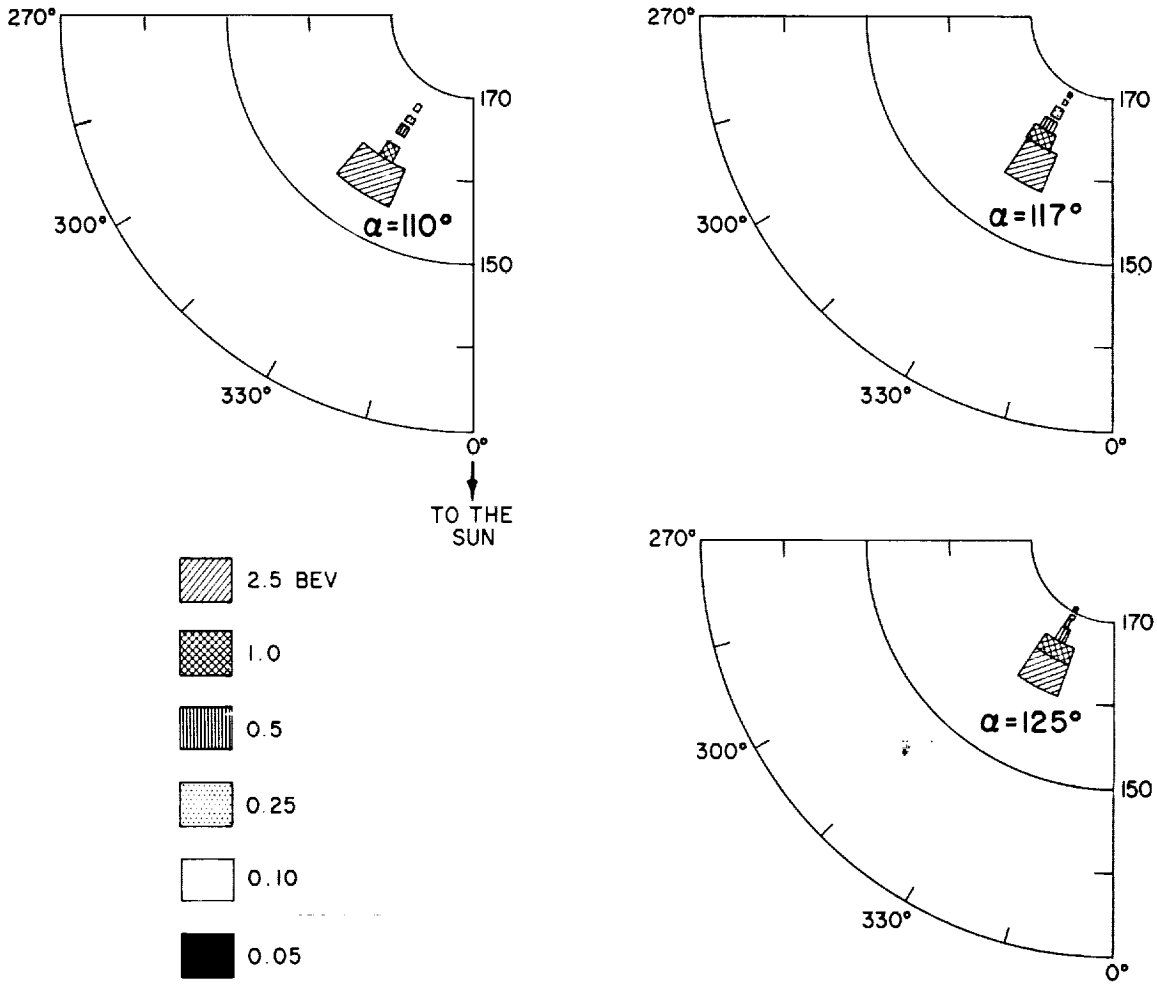

Figure 17 - Impact zones in the Southern Geomagnetic Hemisphere for 0.05 through 2.5 Bev protons when the impact angle $\psi \leq 90°$. (See also Figures 15 and 16.)

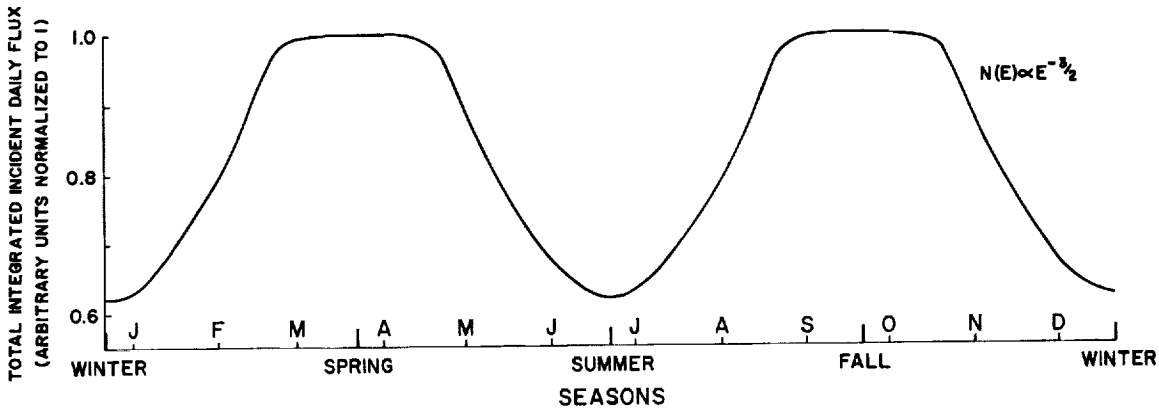

Figure 18 - The total incident daily flux integrated over the whole earth versus season for the energy spectra $N(E) \propto E^{-\frac{3}{2}}$. (See also Figure 19.)

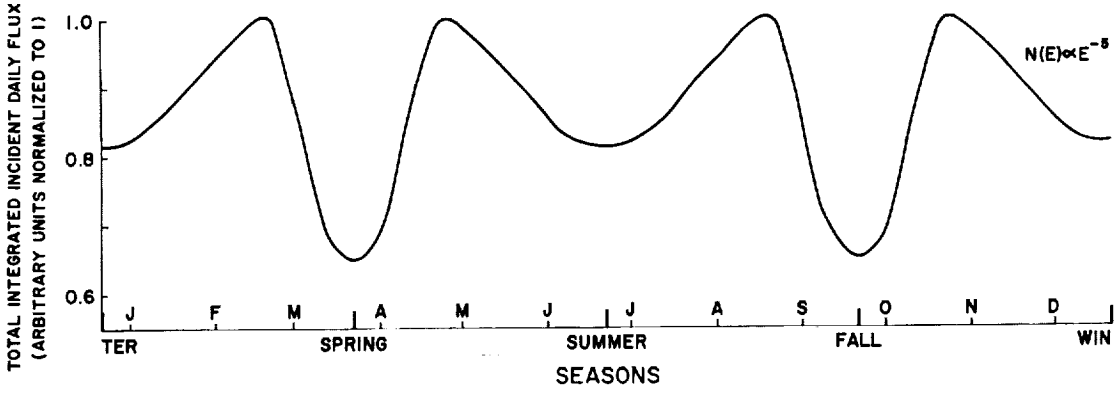

Figure 19 - The total incident daily flux integrated over the whole earth versus season for the energy spectra $N(E) \propto E^{-5}$. (See also Figure 18.)

Table 6

Counting Rates of Protons with Impact Angles ≤ 45° at the Earth's Surface in Blocks 10° Geomagnetic Longitude (ϕ) × 10° Geomagnetic Colatitude (θ) for a Flat Energy Spectrum Beam Incident on the AB Plane

$\alpha = 90°$

Northern Hemisphere

ϕ	θ								Totals
	10 20	20 30	30 40	40 50	50 60	60 70	70 80	80 90	
0-10 50 Bev							3.0	3.0	6.0
20-30 5 Bev				1.7	1.7				3.4
30-40 10 Bev						3.6			3.6
50-60 5 Bev 2.5				1.7 2.9					1.7 2.9
70-80 5 Bev					1.7				1.7
110-120 5 Bev 2.5 1.0			5.7	3.3 2.9					3.3 2.9 5.7
130-140 10 Bev					3.6	3.6			7.2
140-150 25 Bev								6.0	6.0
150-160 5 Bev 2.5 1.0			5.7	2.9	1.7				1.7 2.9 5.7
160-170 25 Bev 10						3.6		6.0	6.0 3.6
170-180 25 Bev								6.0	6.0
190-200 25 Bev 10						3.6	6.0		6.0 3.6
200-210 10 Bev 5				10.6	6.9	10.7			10.7 17.5
210-220 25 Bev 10 5 2.5 1.0			5.9 5.7	26.5 2.9	14.2 5.3	3.6		6.0	6.0 17.8 31.8 8.8 5.7
220-230 25 Bev 10 5 2.5 1.0 0.5 0.25 0.10 0.05		8.9 13.3 21.8 31.2	5.9 5.7	21.2	14.2			18.0	18.0 14.2 21.2 5.9 5.7 8.9 13.3 21.8 31.2

ϕ	θ								Totals
	10 20	20 30	30 40	40 50	50 60	60 70	70 80	80 90	
230-240 25 Bev 10					10.7			6.0	6.0 10.7
240-250 25 Bev 2.5				2.9				18.0	18.0 2.9
250-260 25 Bev								24.0	24.0
260-270 25 Bev 5				1.6				29.9	29.9 1.6
270-280 50 Bev 25						6.0	3.0 18.0	9.1 18.0	12.1 42.0
280-290 50 Bev 25 5 2.5 1.0 0.5		8.9	11.4	6.0 1.7 5.9	3.0 12.0 1.7	6.1 23.9	9.1 12.0	6.1 6.0	24.3 59.9 3.4 5.9 11.4 8.9
290-300 50 Bev 25				3.0 12.0	6.1 12.0	6.1 12.0	6.1 12.0	6.1 12.0	27.4 60.0
300-310 50 Bev 25			12.0	3.0 6.0	6.1 12.0	9.1 12.0	9.1 6.0	6.1 12.0	33.4 60.0
310-320 50 Bev' 25 10 5 2.5 1.0 0.5 0.25 0.10 0.05	26.6 21.8 31.2	52.8 28.6 17.8	6.0 28.5 59.5	6.1 12.0 10.7	6.1 6.0	6.1 6.0	9.1 12.0	9.1 6.0	33.5 48.0 39.2 59.5 52.8 28.6 17.8 26.6 21.8 31.2
320-330 50 Bev 25 10 5		6.6	6.0 49.8 6.6	6.1 6.0	3.0 6.0	9.1 12.0	6.1 6.0	6.1 6.0	30.4 42.0 49.8 13.2
330-340 50 Bev 25			6.0	3.0 6.0	9.1 6.0	6.1 6.0	12.2 6.0	3.0 6.0	33.4 36.0
340-350 50 Bev				6.1	6.1	3.0	6.1	6.1	27.4
350-360 50 Bev				3.0	3.0	6.1	12.2	6.1	30.4

Table 7

Counting Rates of Protons with Impact Angles $\leq 45°$ at the Earth's Surface in Blocks 10° Geomagnetic Longitude (ϕ) × 10° Geomagnetic Colatitude (θ) for a Flat Energy Spectrum Beam Incident on the AB Plane

$\alpha = 90°$

Southern Hemisphere

ϕ	θ
	90
	100
0-10	
50 Bev	9.1
140-150	
25 Bev	6.0
160-170	
25 Bev	6.0
170-180	
25 Bev	6.0
210-220	
25 Bev	6.0
220-230	
25 Bev	18.0
230-240	
25 Bev	6.0
240-250	
25 Bev	18.0
250-260	
25 Bev	23.9
260-270	
25 Bev	29.9
270-280	
50 Bev	12.2
25	18.0

ϕ	θ
	90
	100
280-290	
50 Bev	9.1
25	12.0
290-300	
50 Bev	9.1
25	18.0
300-310	
50 Bev	9.1
25	18.0
310-320	
50 Bev	9.1
25	12.0
320-330	
50 Bev	12.2
25	12.0
330-340	
50 Bev	6.1
25	12.0
340-350	
50 Bev	12.2
350-360	
50 Bev	9.1

Table 8

Counting Rates of Protons with Impact Angles ≤45° at the Earth's Surface in Blocks 10° Geomagnetic Longitude (φ) × 10° Geomagnetic Colatitude (θ) for a Flat Energy Spectrum Beam Incident on the AB Plane

$\alpha = 100°$

Northern Hemisphere

φ	θ								Totals
	10 20	20 30	30 40	40 50	50 60	60 70	70 80	80 90	
0-10 50 Bev							3.0	3.0	6.0
30-40 10 Bev							3.6		3.6
50-60 10 Bev							3.6		3.6
100-110 10 Bev					3.6				3.6
160-170 10 Bev						3.6			3.6
200-210 25 Bev							6.0		6.0
210-220 25 Bev 10						10.7	12.0	18.0	30.0 10.7
220-230 10 Bev 5				19.8	10.7	7.1			17.8 19.8
230-240 25 Bev 10 5 2.5 1.0 0.5		17.8	23.5 22.9	19.8	21.4	3.6	12.0	12.0	24.0 25.0 19.8 23.5 22.9 17.8
240-250 25 Bev 10 5 2.5 1.0			2.9 5.7	6.6	17.8		29.9	6.0	35.9 17.8 6.6 2.9 5.7
250-260 25 Bev 10				7.1	7.1		23.9		23.9 14.2

φ	θ								Totals
	10 20	20 30	30 40	40 50	50 60	60 70	70 80	80 90	
270-280 50 Bev 25						18.0	3.0 18.0	9.1 18.0	12.1 54.0
280-290 50 Bev 25				6.0	3.0 12.0	6.1 18.0	9.1 12.0	6.1 12.0	24.3 60.0
290-300 50 Bev 25			6.0	6.0	3.0 12.0	6.1 6.0	6.1 12.0	9.1 12.0	24.3 54.0
300-310 50 Bev 25 10 5 2.5 1.0 0.5 0.25 0.10 0.5	21.8 31.2	11.7 28.6 26.7 26.7	52.9 41.0	3.0 12.0 39.2	3.0 12.0	6.1 12.0	6.1 6.0	6.1 12.0	24.3 54.0 39.2 52.9 52.7 28.6 26.7 26.7 21.8 31.2
310-320 50 Bev 25 10 5 2.5			6.0 7.1 26.5 5.9	3.0 6.0 64.1	3.0 6.0	6.1 12.0	9.1 6.0	6.1 12.0	27.3 48.0 71.2 26.5 5.9
320-330 50 Bev 25				6.0	3.0 6.0	9.1 12.0	9.1 6.0	12.2 12.0	33.4 42.0
330-340 50 Bev					6.1	6.1	6.1	3.0	21.3
340-350 50 Bev					3.0	3.0	12.2	6.1	24.3
350-360 50 Bev 10						3.0 3.6	6.1	3.0	12.1 3.6

Table 9

Counting Rates of Protons with Impact Angles ≤ 45° at the Earth's Surface in Blocks 10° Geomagnetic Longitude (ϕ) × 10° Geomagnetic Colatitude (θ) for a Flat Energy Spectrum Beam Incident on the AB Plane

$\alpha = 100°$

Southern Hemisphere

ϕ	θ								Totals
	90	100	110	120	130	140	150	160	
	100	110	120	130	140	150	160	170	
0-10									
50 Bev	9.1	6.1	6.1	3.0					24.3
20-30									
10 Bev			3.6						3.6
30-40									
10 Bev				3.6					3.6
120-130									
10 Bev		3.6							3.6
130-140									
10 Bev				3.6					3.6
140-150									
10 Bev						3.6			3.6
5				6.6	6.6				13.2
2.5					2.9				2.9
1.0						5.7			5.7
0.5							8.9		8.9
170-180									
10 Bev		3.6	3.6						7.2
180-190									
10 Bev			3.6						3.6
5				6.6					6.6
2.5					2.9				2.9
190-200									
10 Bev			10.7						10.7
5				6.6	13.2				19.8
2.5					5.9				5.9
1.0						5.7			5.7
200-210									
10 Bev				14.2					14.2
5					13.2				13.2
2.5					2.9	5.9			8.8
1.0						5.7			5.7
0.5							8.9		8.9
0.25							13.3		13.3
210-220									
10 Bev				10.7					10.7

ϕ	θ								Totals
	90	100	110	120	130	140	150	160	
	100	110	120	130	140	150	160	170	
270-280									
50 Bev	6.1	3.0	3.0						12.1
25	6.0								6.0
280-290									
50 Bev	9.1	6.1	12.2	6.1					33.5
25	12.0	18.0	6.0						36.0
2.5					2.9				2.9
1.0						5.7			5.7
290-300									
50 Bev	6.1	6.1	6.1	6.1	6.1				30.5
25	12.0	18.0	12.0	12.0	12.0	6.0			72.0
300-310									
50 Bev	9.1	6.1	9.1	6.1	6.1	6.1			42.6
25	12.0	12.0	6.0	12.0	6.0	6.0			54.0
5					6.6				6.6
310-320									
50 Bev	9.1	9.1	9.1	6.1	6.1	3.0			42.5
25	12.0	6.0	12.0	12.0	6.0	12.0	6.0		66.0
5						6.6			6.6
2.5							2.9		2.9
320-330									
50 Bev	6.1	6.1	9.1	9.1	3.0	3.0			36.4
25	6.0	12.0	6.0	12.0					48.0
10						89.0			89.0
5						6.6	46.3		52.9
2.5							41.0		41.0
1.0							28.6		28.6
0.5								33.6	33.6
0.25								26.6	26.6
0.10								21.8	21.8
330-340									
50 Bev	6.1	12.1	6.1	6.1	6.1	6.1			42.6
25	6.0	6.0	6.0	6.0	6.0	6.0	6.0		42.0
340-350									
50 Bev	12.2	6.1	6.1	3.0	6.1	6.1			39.6
25			6.0		6.0	6.0			18.0
350-360									
50 Bev	6.1	6.1	9.1	3.0	6.1	3.0			33.4

Table 10

Counting Rates of Protons with Impact Angles ≤ 45° at the Earth's Surface in Blocks 10° Geomagnetic Longitude (ϕ) × 10° Geomagnetic Colatitude (θ) for a Flat Energy Spectrum Beam Incident on the AB Plane

$\alpha = 110°$

Northern Hemisphere

ϕ	θ								Totals
	10 20	20 30	30 40	40 50	50 60	60 70	70 80	80 90	
0–10 50 Bev								3.0	3.0
50–60 10 Bev						3.6			3.6
100–110 10 Bev						3.6			3.6
220–230 25 Bev						12.0			12.0
230–240 25 Bev 10					7.1	18.0 3.6	6.0		24.0 10.7
240–250 25 Bev 10 5				26.5	21.4	6.0			6.0 21.4 26.5
250–260 25 Bev 10 5 2.5			37.5	3.6 19.8	35.6	23.9			23.9 39.2 19.8 37.5
260–270 25 Bev 10 5 2.5 1.0 0.5 0.25		54.9 85.4 42.6	84.4 54.9	14.2 33.1	6.0 28.5	29.9			35.9 42.7 33.1 84.4 109.8 85.4 42.6
270–280 25 Bev 10 5 2.5 1.0 0.5 0.25 0.10		109.8 142.4 85.1 69.8	103.2 18.3	24.9 52.9	18.0 24.9	18.0	6.0		42.0 49.8 52.9 103.2 128.1 142.4 85.1 69.8

ϕ	θ								Totals
	10 20	20 30	30 40	40 50	50 60	60 70	70 80	80 90	
280–290 50 Bev 25 10 5 2.5 1.0 0.5 0.25		146.4 142.4 170.3	26.5 122.0	6.0 46.3 33.1	12.0 24.9	12.0	6.1	9.1	15.2 30.0 71.2 59.6 122.0 146.4 142.4 170.3
290–300 50 Bev 25 10 5 2.5			59.6 37.5	6.0 89.0	18.0 7.1	3.0 18.0	6.1 6.0	6.1	15.2 48.0 96.1 59.6 37.5
300–310 50 Bev 25 10				6.0 17.8	6.0	3.0 12.0	6.1 6.0	6.1 6.0	15.2 36.0 17.8
310–320 50 Bev						6.1	6.1	6.1	18.3
320–330 50 Bev						3.0	9.1	12.2	24.3
330–340 50 Bev							6.1	3.0	9.1
340–350 50 Bev							9.1	9.1	18.2
350–360 50 Bev								6.1	6.1

Table 11

Counting Rates of Protons with Impact Angles ≤45° at the Earth's Surface in Blocks 10° Geomagnetic Longitude (ϕ) × 10° Geomagnetic Colatitude (θ) for a Flat Energy Spectrum Beam Incident on the AB Plane

$\alpha = 110°$

Southern Hemisphere

ϕ	θ								Totals
	90	100	110	120	130	140	150	160	
	100	110	120	130	140	150	160	170	
0-10									
50 Bev	3.0	3.0	6.1	6.1	6.1	3.0			27.3
10-20									
50 Bev			3.0	3.0					6.0
140-150									
10 Bev			3.6						3.6
150-160									
10 Bev				3.6					3.6
160-170									
10 Bev			3.6	7.1					10.7
5					13.2				13.2
170-180									
10 Bev			3.6	21.4					25.0
180-190									
10 Bev			3.6	3.6					7.2
190-200									
10 Bev				10.7					10.7
240-250									
10 Bev				3.6					3.6
280-290									
50 Bev		12.2	3.0	6.1	6.1				27.4
290-300									
50 Bev	9.1	6.1	6.1	9.1	6.1	6.1			42.6
25			12.0	12.0	12.0	6.0			42.0

ϕ	θ								Totals
	90	100	110	120	130	140	150	160	
	100	110	120	130	140	150	160	170	
300-310									
50 Bev	9.1	6.1	9.1	6.1	6.1	6.1			42.6
25	6.0	6.0	18.0	6.0	12.0	12.0	6.0		66.0
310-320									
50 Bev	9.1	6.1	9.1	6.1	3.0	3.0	3.0		39.4
25	6.0	12.0	6.0	6.0	12.0				42.0
10						21.4	7.1		28.5
320-330									
50 Bev	9.1	6.1	6.1	9.1	6.1	6.1	3.0		45.6
25		12.0	6.0	6.0	12.0	12.0	6.0		54.0
10						21.4	28.5		49.0
5							33.1		33.1
2.5							75.1		75.1
1.0								34.3	34.3
0.5								17.8	17.8
0.25								26.6	26.6
330-340									
50 Bev	6.1	12.2	6.1	6.1	3.0	6.1	3.0		42.5
25			12.0	12.0	6.0	6.0			36.0
5							24.5		24.5
2.5							9.4		9.4
340-350									
50 Bev	9.1	6.1	9.1	3.0	6.1	6.1			39.5
25				6.0	6.0	6.0	6.0		24.0
350-360									
50 Bev	3.0	12.2	6.1	6.1	3.0	3.0	3.0		36.4
25						6.0			6.0

Table 12

Counting Rates of Protons with Impact Angles $\leq 45°$ at the Earth's Surface in Blocks $10°$ Geomagnetic Longitude (ϕ) $\times$ $10°$ Geomagnetic Colatitude (θ) for a Flat Energy Spectrum Beam Incident on the AB Plane

$\alpha = 117°$

Northern Hemisphere

Φ	θ								Totals
	10	20	30	40	50	60	70	80	
	20	30	40	50	60	70	80	90	
240–250									
25 Bev					6.0	6.0			12.0
250–260									
25 Bev					6.0				6.0
10					10.6				10.6
260–270									
25 Bev					18.0				18.0
10					39.2				39.2
270–280									
25 Bev					6.0				6.0
10				10.7	32.0				42.7
280–290									
25 Bev				6.0					6.0
10				7.1	7.1				14.2

Φ	θ								Totals
	10	20	30	40	50	60	70	80	
	20	30	40	50	60	70	80	90	
290–300									
50 Bev								9.1	9.1
300–310									
50 Bev							3.0	6.1	9.1
310–320									
50 Bev							6.1	3.0	9.1
320–330									
50 Bev							3.0	6.1	9.1
330–340									
50 Bev								12.2	12.2
340–350									
50 Bev								3.0	3.0
350–360									
50 Bev								3.0	3.0

Table 13

Counting Rates of Protons with Impact Angles $\leq 45°$ at the Earth's Surface in Blocks 10° Geomagnetic Longitude (ϕ) × 10° Geomagnetic Colatitude (θ) for a Flat Energy Spectrum Beam Incident on the AB Plane

$\alpha = 117°$

Southern Hemisphere

ϕ	θ								Totals
	90	100	110	120	130	140	150	160	
	100	110	120	130	140	150	160	170	
0-10									
50 Bev		3.0	6.1	3.0	6.1	3.0	3.0		24.2
10-20									
50 Bev			3.0	3.0	6.1	3.0			15.1
280-290									
50 Bev		3.0	3.0	6.1	3.0	6.1			21.2
290-300									
50 Bev	3.0	6.1	9.1	6.1	6.1	3.0			33.4
300-310									
50 Bev	9.1	6.1	9.1	6.1	3.0	6.1	6.1		45.6
25			6.0	18.0	6.0	12.0	6.0		48.0
310-320									
50 Bev	9.1	9.1	9.1	6.1	9.1	3.0	3.0		48.5
25			6.0	12.0	6.0	12.0	12.0		48.0
320-330									
50 Bev	9.1	6.1	6.1	9.1	3.0	3.0	3.0		39.4
25			12.0	12.0	6.0	6.0			36.0
10							3.6		3.6
5							23.2		23.2
2.5							11.7	7.0	18.7
1.0								18.3	18.3
0.5								7.1	7.1
0.25								21.3	21.3

ϕ	θ								Totals
	90	100	110	120	130	140	150	160	
	100	110	120	130	140	150	160	170	
330-340									
50 Bev	3.0	12.2	6.1	6.1	9.1	6.1	3.0	3.0	48.6
25				6.0	12.0	6.0	6.0	6.0	36.0
10							85.4		85.4
5							34.7		34.7
2.5							46.9	9.4	56.3
1.0								36.6	36.6
0.5								42.7	42.7
0.25								21.3	21.3
0.10								34.9	34.9
0.05								25.0	25.0
340-350									
50 Bev	12.2	3.0	9.1	6.1	6.1	3.0	3.0		39.5
25				6.0	6.0	6.0			18.0
350-360									
50 Bev	3.0	9.1	6.1	9.1	3.0	6.1	3.0		39.4
25						6.0	6.0		12.0

Table 14

Counting Rates of Protons with Impact Angles $\leq 45°$ at the Earth's Surface in Blocks 10° Geomagnetic Longitude (ϕ) × 10° Geomagnetic Colatitude (θ) for a Flat Energy Spectrum Beam Incident on the AB Plane

$\alpha = 125°$

Southern Hemisphere

ϕ	θ								Totals
	90	100	110	120	130	140	150	160	
	100	110	120	130	140	150	160	170	
0-10									
50 Bev			9.1	3.0	9.1	3.0	6.1		30.3
25							6.0		6.0
10-20									
50 Bev			3.0	6.1	3.0	6.1		3.0	21.2
20-30									
50 Bev						3.0	3.0		6.0
280-290									
50 Bev				3.0	3.0	6.1		3.0	15.1
290-300									
50 Bev		3.0	6.1	9.1	3.0	3.0	6.1		30.3
25						12.0			12.0
300-310									
50 Bev		9.1	6.1	9.1	3.0	6.1	3.0		36.4
25				6.0	12.0	6.0	12.0		36.0
310-320									
50 Bev	6.1	9.1	6.1	6.1	9.1	3.0	6.1	3.0	48.6
25				6.0	6.0	6.0		6.0	24.0
320-330									
50 Bev	9.1	6.1	12.2	6.1	3.0	3.0	3.0		42.5
25				6.0	6.0	12.0	6.0	6.0	36.0
5							13.2	3.3	16.5
2.5								9.4	9.4
1.0								4.6	4.6

ϕ	θ								Totals
	90	100	110	120	130	140	150	160	
	100	110	120	130	140	150	160	170	
330-340									
50 Bev	9.1	6.1	6.1	6.1	9.1	6.1	3.0	3.0	48.6
25				6.0	6.0	12.0			24.0
10							85.4		85.4
5							21.5	21.5	43.0
2.5								63.3	63.3
1.0								45.8	45.8
0.5								35.6	35.6
0.25								42.6	42.6
0.10								52.4	52.4
								θ	
								170	
								180	
0.05								25.0	25.0
340-350									
50 Bev	6.1	6.1	9.1	3.0	9.1		6.1		39.5
25					6.0	6.0	6.0		24.0
350-360									
50 Bev		6.1	6.1	6.1	3.0	3.0	3.0		27.3
25					6.0		6.0		12.0

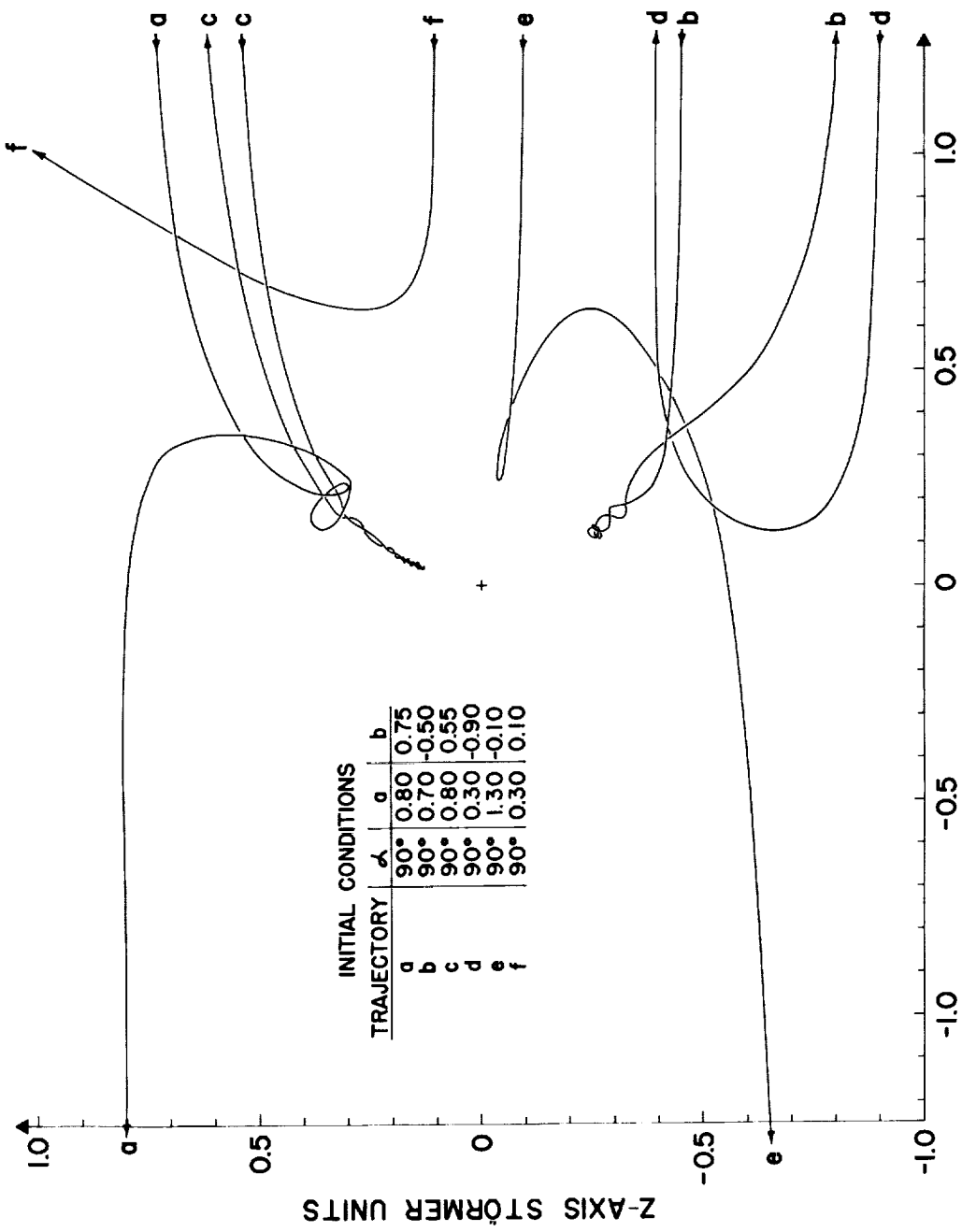

Figure 20 - Example trajectory for dayside conditions. (See also Figure 21.)

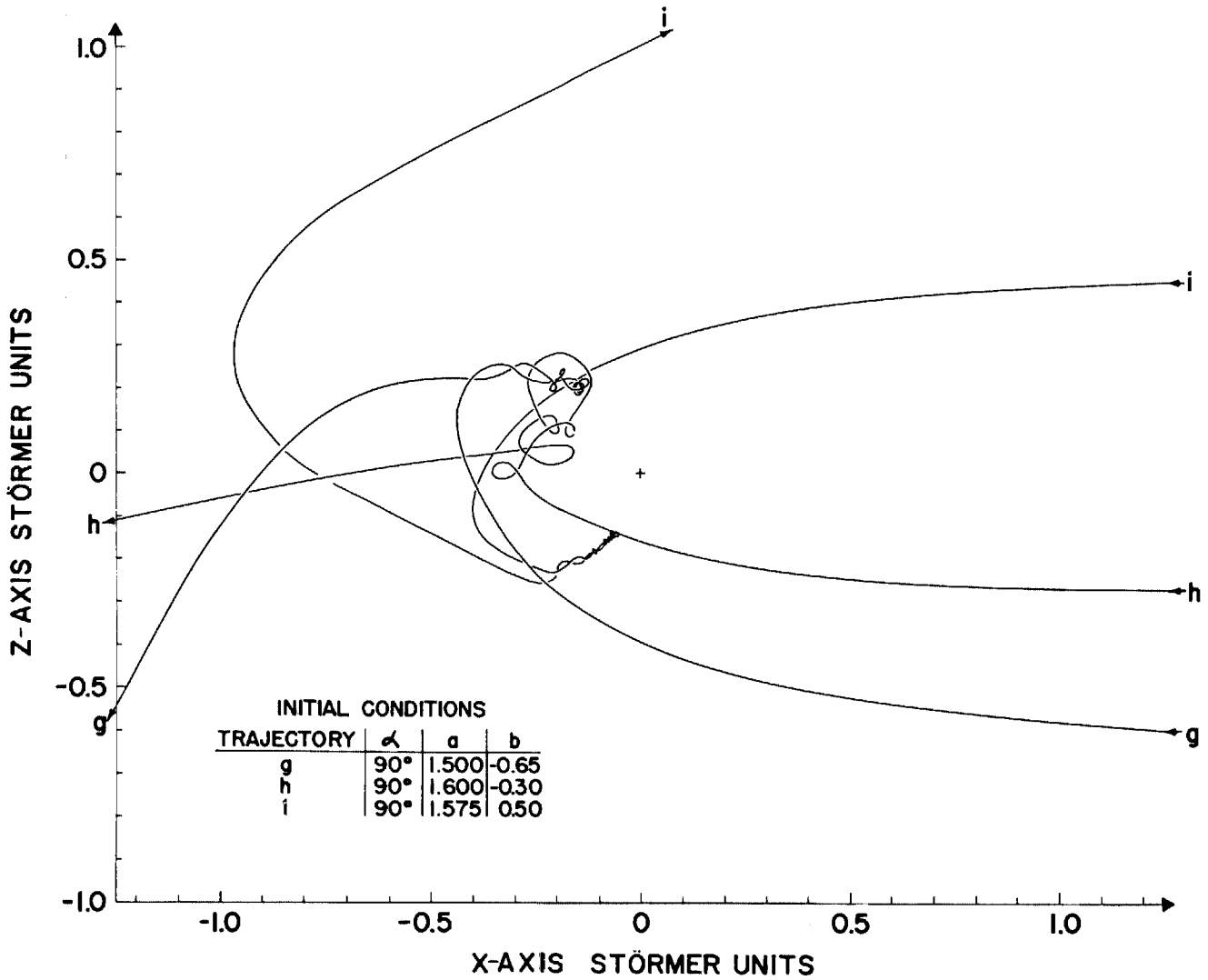

Figure 21 - Example trajectory for nightside conditions. (See also Figure 20.)

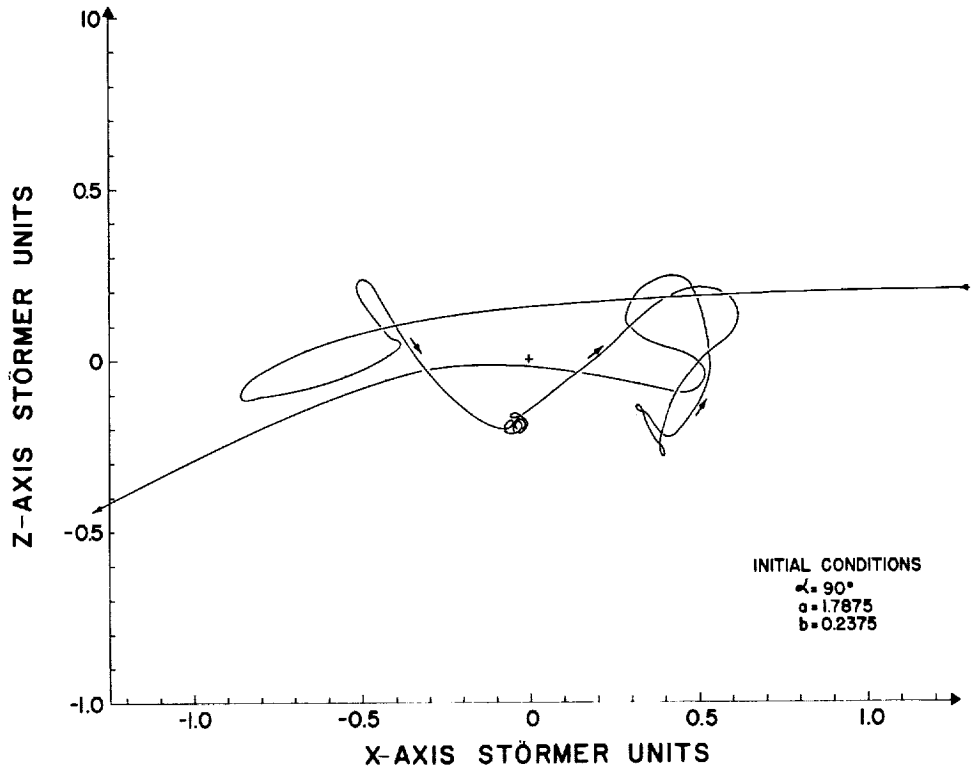

Figure 22 - A simple quasi-trapped trajectory. (See also Figure 23.)

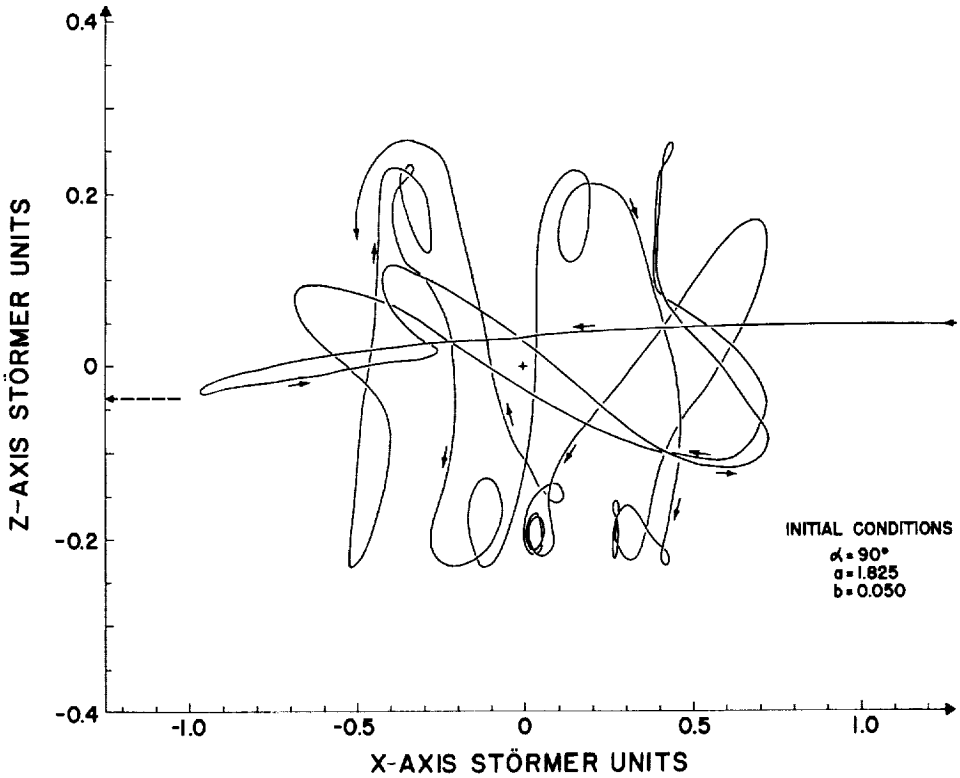

Figure 23 - A complicated quasi-trapped trajectroy. (See also Figure 22.)

ACKNOWLEDGMENTS

The author is grateful to Dr. Robert Jastrow for proposing this investigation and to Drs. Jastrow and C. A. Pearse for many valuable discussions. He also thanks Mrs. L. Shapiro of the Naval Research Laboratory and Miss M. Pinker of Naval Proving Grounds for preparing the machine programs for these calculations.

REFERENCES

1. Störmer, C., "On the Trajectories of Electric Particles in the Field of a Magnetic Dipole with Applications to the Theory of Cosmic Radiation," Astrophysica Norvegica 1(1): 1-10, June 1934
2. Lemaitre, G., and Vallarta, M. S., "On the Geomagnetic Analysis of Cosmic Radiation," Phys. Rev. 49(10):719-726, May 15, 1936
3. Dwight, K., "Solar Magnetic Moment and Diurnal Variation in Intensity of Cosmic Radiation," Phys. Rev. 78(1):40-49, April 1, 1950
4. Schlüter, A., "Solare Ultrastrahlung and Erdmagnetfeld," Zeitschrift für Naturforschung 6a(11):613-618, November 1951
5. Firor, J., "Cosmic Radiation Intensity-Time Variations and Their Origin. IV. Increases Associated with Solar Flares," Phys. Rev. 94(4):1017-1028, May 15, 1954
6. Lüst, R., Schlüter, A. and Katterbach, K., "Die Bahnen von Teilchen der Kosmischen Strahlung im Erdmagnetfeld," Nachr. Akad. Wiss. Göttingen, Math.-Phys. Kl., Abt. IIa, no. 8:127-223, 1955
7. Jory, F. S., "Selected Cosmic-Ray Orbits in the Earth's Magnetic Field," Phys. Rev. 103(4):1068-1075, August 15, 1956
8. Lüst, R., "Impact Zones for Solar Cosmic-Ray Particles," Phys. Rev. 105(6):1827-1839, March 15, 1957
9. Birkeland, Kr., "Expeditions Norvegiennes de 1899-1900 pour l'Etude des Aurores Boreales. Resultats des Recherches Magnetiques," Skr. Vidensk.-Selsk., Christiania, Mat.-Naturv. Kl. paper no. 1, 1901
10. Malmfors, K. G., "Determination of Orbits in the Field of a Magnetic Dipole with Applications to the Theory of the Diurnal Variation of Cosmic Radiation," Ark. Mat. Astr. Fys. 32A, paper no. 8, 1945
11. Brunberg, E., and Dattner, A., "Experimental Determination of Electron Orbits in the Field of a Magnetic Dipole," Tellus 5(2):135-156, May 1953
12. Bennett, W. H., "Solar Proton-Stream Forms as Related to the Aurorae," J. Geophys. Res. 61(2) part 2, pp. 359, June 1956

13. Montgomery, D.J.X., "Cosmic Ray Physics," Princeton: Princeton University Press, 1949

14. Rothwell, P., and Quenby, J., "Cosmic Rays in the Earth's Magnetic Field," Nuovo Cimento, Suppl. No. 2 to Vol. 8, Series 10: 249-256, 1958

15. Katz, L., Meyer, P., and Simpson, J. A., "Further Experiments Concerning the Geomagnetic Field Effective for Cosmic Rays," Nuovo Cimento, Suppl. No. 2 to Vol. 8, Series 10: 277-282, 1958

NASA TN D-1291
National Aeronautics and Space Administration.
SOLAR PROTON IMPACT ZONES. Thomas Kelsall.
June 1962. 33p. OTS price, $1.00.
(NASA TECHNICAL NOTE D-1291)

The trajectories of charged particles moving in a magnetic dipole field have been calculated by numerical integration for application to data on the intensity variation of cosmic rays during recent solar events. All seasons and times of day have been covered by assuming a range of orientations of the incident particle beam with respect to the magnetic dipole axis. The points of impact with the earth have been determined for protons with energies from 0.05 to 50 Bev. The computation includes 4000 trajectories and fills several gaps in previous investigations. In agreement with earlier calculations the results indicate that the protons strike in well defined areas between 0 and 1200 hours local time and are focused into small areas of impact at low energies. The investigation

(over)

I. Kelsall, Thomas
II. NASA TN D-1291

(Initial NASA distribution:
6, Astronomy;
7, Astrophysics;
21, Geophysics and geodesy.)

NASA

NASA TN D-1291
National Aeronautics and Space Administration.
SOLAR PROTON IMPACT ZONES. Thomas Kelsall.
June 1962. 33p. OTS price, $1.00.
(NASA TECHNICAL NOTE D-1291)

The trajectories of charged particles moving in a magnetic dipole field have been calculated by numerical integration for application to data on the intensity variation of cosmic rays during recent solar events. All seasons and times of day have been covered by assuming a range of orientations of the incident particle beam with respect to the magnetic dipole axis. The points of impact with the earth have been determined for protons with energies from 0.05 to 50 Bev. The computation includes 4000 trajectories and fills several gaps in previous investigations. In agreement with earlier calculations the results indicate that the protons strike in well defined areas between 0 and 1200 hours local time and are focused into small areas of impact at low energies. The investigation

(over)

I. Kelsall, Thomas
II. NASA TN D-1291

(Initial NASA distribution:
6, Astronomy;
7, Astrophysics;
21, Geophysics and geodesy.)

NASA

NASA TN D-1291
National Aeronautics and Space Administration.
SOLAR PROTON IMPACT ZONES. Thomas Kelsall.
June 1962. 33p. OTS price, $1.00.
(NASA TECHNICAL NOTE D-1291)

The trajectories of charged particles moving in a magnetic dipole field have been calculated by numerical integration for application to data on the intensity variation of cosmic rays during recent solar events. All seasons and times of day have been covered by assuming a range of orientations of the incident particle beam with respect to the magnetic dipole axis. The points of impact with the earth have been determined for protons with energies from 0.05 to 50 Bev. The computation includes 4000 trajectories and fills several gaps in previous investigations. In agreement with earlier calculations the results indicate that the protons strike in well defined areas between 0 and 1200 hours local time and are focused into small areas of impact at low energies. The investigation

(over)

I. Kelsall, Thomas
II. NASA TN D-1291

(Initial NASA distribution:
6, Astronomy;
7, Astrophysics;
21, Geophysics and geodesy.)

NASA

NASA TN D-1291
National Aeronautics and Space Administration.
SOLAR PROTON IMPACT ZONES. Thomas Kelsall.
June 1962. 33p. OTS price, $1.00.
(NASA TECHNICAL NOTE D-1291)

The trajectories of charged particles moving in a magnetic dipole field have been calculated by numerical integration for application to data on the intensity variation of cosmic rays during recent solar events. All seasons and times of day have been covered by assuming a range of orientations of the incident particle beam with respect to the magnetic dipole axis. The points of impact with the earth have been determined for protons with energies from 0.05 to 50 Bev. The computation includes 4000 trajectories and fills several gaps in previous investigations. In agreement with earlier calculations the results indicate that the protons strike in well defined areas between 0 and 1200 hours local time and are focused into small areas of impact at low energies. The investigation

(over)

I. Kelsall, Thomas
II. NASA TN D-1291

(Initial NASA distribution:
6, Astronomy;
7, Astrophysics;
21, Geophysics and geodesy.)

NASA

NASA TN D-1291

has shown two facts which are not new, but which have received relatively little attention in earlier work. First, the relative number of impacts in the northern and southern geomagnetic hemispheres is strongly dependent on season. Second, under certain conditions of season there is a class of trajectories which may be called quasi-trapped, consisting of a set of paths which resemble the trapped trajectories first discovered by Störmer but which are connected to infinity. It is suggested that injection into trapped orbits from these quasi-trapped trajectories may make a contribution to the population of the Van Allen belts.

NASA

NASA TN D-1291

has shown two facts which are not new, but which have received relatively little attention in earlier work. First, the relative number of impacts in the northern and southern geomagnetic hemispheres is strongly dependent on season. Second, under certain conditions of season there is a class of trajectories which may be called quasi-trapped, consisting of a set of paths which resemble the trapped trajectories first discovered by Störmer but which are connected to infinity. It is suggested that injection into trapped orbits from these quasi-trapped trajectories may make a contribution to the population of the Van Allen belts.

NASA

NASA TN D-1291

has shown two facts which are not new, but which have received relatively little attention in earlier work. First, the relative number of impacts in the northern and southern geomagnetic hemispheres is strongly dependent on season. Second, under certain conditions of season there is a class of trajectories which may be called quasi-trapped, consisting of a set of paths which resemble the trapped trajectories first discovered by Störmer but which are connected to infinity. It is suggested that injection into trapped orbits from these quasi-trapped trajectories may make a contribution to the population of the Van Allen belts.

NASA

NASA TN D-1291

has shown two facts which are not new, but which have received relatively little attention in earlier work. First, the relative number of impacts in the northern and southern geomagnetic hemispheres is strongly dependent on season. Second, under certain conditions of season there is a class of trajectories which may be called quasi-trapped, consisting of a set of paths which resemble the trapped trajectories first discovered by Störmer but which are connected to infinity. It is suggested that injection into trapped orbits from these quasi-trapped trajectories may make a contribution to the population of the Van Allen belts.

NASA